DOI 10.1007/978-1-4939-3547-5_11
Reprinted from *Space Science Reviews* Journal, DOI 10.1007/s11214-014-0126-7

Current Sheets in the Earth Magnetotail: Plasma and Magnetic Field Structure with Cluster Project Observations

Anatoli Petrukovich · Anton Artemyev · Ivan Vasko · Rumi Nakamura · Lev Zelenyi

Received: 17 October 2014 / Accepted: 8 December 2014 / Published online: 7 February 2015

Abstract Thin current sheets having kinetic scales are an important plasma structure, where the magnetic energy dissipation and charged particle acceleration are the most effective. It is believed that such current sheets are self-consistently formed by the specific nonadiabatic dynamics of charged particles and play a critical role in many space plasma and astrophysical objects. Current sheets in the near-Earth plasma environment, e.g., the magnetotail current sheet, are readily available for *in-situ* investigations. The dedicated multi-spacecraft Cluster mission have revealed basic properties of this current sheet, which are presented in this review: typical spatial profiles of magnetic field and current density, distributions of plasma temperature and density, role of heavy ions and electron currents, etc. Being important for the Earth magnetosphere physics, the new knowledge also could provide the basis for advancement in general plasma physics as well as in plasma astrophysics.

Keywords Current sheet · Planetary magnetospheres · Kinetic plasma structures

1 Introduction

Current sheets (CSs) represent the typical magnetic field configuration in plasmas where the thermal pressure dominates in comparison with the magnetic one (i.e. plasma systems with a large value of plasma β-parameter). CSs are often introduced qualitatively as spatially localized regions, where magnetic field substantially changes the direction or/and amplitude.

A. Petrukovich · A. Artemyev (✉) · I. Vasko · L. Zelenyi
Space Research Institute (IKI), RAS, Moscow, Russia
e-mail: ante0226@gmail.com

A. Petrukovich
e-mail: apetruko@iki.rssi.ru

L. Zelenyi
e-mail: lzelenyi@iki.rssi.ru

R. Nakamura
Space Research Institute (IWF), OAW, Graz, Austria

One can distinguish forced CS formed due to external driving at the boundary of two plasma domains with different properties (e.g. at the magnetopause of the Earth's magnetosphere) and spontaneous CS formed in the course of self-consistent evolution of plasma systems without direct external driving (e.g. magnetotail). CSs play the fundamentally important role because the magnetic energy dissipates within these structures to kinetic energy of accelerated charged particles and thermal plasma energy (Parker 1994; Priest and Forbes 2000; Birn and Priest 2007).

In-situ spacecraft observations have demonstrated that CSs are formed in practically all very different magnetospheres (Jackman et al. 2014): the dynamic and compact Mercury magnetosphere (Slavin et al. 2012), the induced magnetosphere of Venus (Vaisberg and Zeleny 1984; McComas et al. 1986a; Vasko et al. 2014b), the Earth magnetosphere (Ness 1965), the disk-like magnetospheres of Saturn (Dougherty et al. 2009) and Jupiter (Smith et al. 1974; Behannon et al. 1981; Artemyev et al. 2014b), the cylindrically symmetric magnetospheres of Neptune and Uranus (Ness et al. 1989), magnetospheres of comets (McComas et al. 1987), etc. CSs in solar corona represent the critical element of numerous modern solar-flare theories (Aschwanden 2002). In solar wind CSs can also be formed due to the inhomogeneity of solar wind flows (Gosling 2012). Detected radiation of accelerated electrons from pulsar nebulae also points to the possible important role of CS in this exotic system (Arons 2012).

The Earth magnetotail CS is for the obvious reasons the most investigated one. CS with magnetic field reversal is a core part of the plasma sheet—the region with the closed (connected to the Earth ionosphere) magnetic field lines, filled with hot plasmas. According to the modern scenario of magnetospheric disturbances (substorms), the CS structure and stability determines dynamics of the whole magnetotail (Baker et al. 1996).

It is commonly (and erroneously) assumed that the scales of variations of the plasma parameters in space and astrophysical objects are comparable with the scales of these objects. In particular magnetic field and plasma density variations in the magnetotail for many years were supposed to occur on the scale comparable with that of the magnetosphere cross-section, i.e. few tens of 10^3 km (e.g., Bird and Beard 1972; Schindler 1974; Kan 1973; Schindler 1979). On the other hand the classic theory predicts that the most efficient dissipation of magnetic energy in collisionless plasma occurs on kinetic plasma scales within such structures as shock waves, magnetic discontinuities, kinetic current sheets, etc. Kinetic scales (in magnetized plasma controlled by the Larmor radius of the heaviest plasma species) are much smaller than scales of the majority of space plasma objects (e.g., ion Larmor radius in the outer Earth's magnetosphere is one hundred times smaller than the magnetotail diameter).

General plasma characteristics (magnetic field, density, temperature) as well as some geometrical properties of the magnetotail have been successfully investigated with the help of a number of single and double spacecraft missions (OGO, IMP, ISEE, AMPTE, Geotail, Interball-tail) of twentieth century (McComas et al. 1986b; Baumjohann et al. 1989; Mitchell et al. 1990; Sergeev et al. 1993; Hoshino et al. 1996; Petrukovich et al. 1999; Asano et al. 2004b). These observations clearly pointed out that dynamics of the tail CS indeed should be driven by charged particle kinetics and thus strongly depends on the CS spatial profile (e.g., thickness scale). However, determination of spatial scales of magnetic field and plasma structures in the near-Earth domain cannot be solved reliably by the measurements on a single spacecraft.

A four-spacecraft European Cluster mission (since 2000) was specially designed for determination on a regular basis of spatial gradients in the magnetotail on both fluid (10 000 km) and ion kinetic scales (100–1000 km) (Credland et al. 1997; Escoubet et al.

2001). Indeed, many structures with kinetic scales have been found (Sharma et al. 2008). These new observations revealed the multiscale nature of the Earth's magnetotail, in which very thin (∼100–1000 km) current sheets can be responsible for the generation of 50 % of the magnetic field total amplitude. Although, these results are important for the modeling of magnetotail stability and dynamics, they also give lessons on the possible configurations of self-consistent plasma systems. Namely, independently of the general system scale, significant processes (electric current generation, magnetic reconnection, charged particle acceleration, etc.) can occur at kinetic scales where dynamics of relatively small populations of charged particles may drive the whole magnetic field configuration. These properties should be (and can be) taken into account in the CS theoretical models and simulations.

There are several aspects of magnetotail CS structure, which we would like to discuss below in this paper:

1. Statistics of current sheet thicknesses, i.e. scales of magnetic field inhomogeneities in the vicinity of the magnetotail central region and its relation to plasma spatial scales (ion gyroradious, ion inertial length).
2. Relation between thicknesses of the plasma sheet and CS, spatial gradients of density and temperature.
3. The role of heavy ions in the sheet structure (in addition to protons and electrons).
4. Underlying physics of the electric current (diamagnetic drift of hot ions, non-adiabatic ions, Hall electric field, etc.).
5. Vertical current sheets as newly discovered dynamical structures.
6. Formation of thin current sheets and their two-dimensional configuration (including gradients along the tail)

2 Models of Current Sheets

In this section we give a brief review of CS models. Although, there is a large number of analytical and numerical MHD models of CS (Bird and Beard 1972; Birn et al. 1975; Birn 1979; Schindler and Birn 1986; Whipple et al. 1991; Steinhauer et al. 2008) we concentrate here on kinetic models, which allow to describe structures, comparable with ion scales and which represent self-consistent solutions of Vlasov–Maxwell equations (Schindler 2006). We use the GSM coordinate system: X axis is directed from the Earth to the Sun, Z axis is in the plane, containing X-axis and Earth magnetic moment, Y axis completes the right-handed coordinate system. For a typical (horizontal) sheet the normal as well as the main inhomogeneity scale are directed almost along Z (hereafter called vertical structure), electric current is along Y. Weaker gradients in the magnetotail are possible along X (tail axis).

The simplest CS model which has been widely used for description of spacecraft observations was proposed by Harris (1962). This self-consistent model describes 1D CS with the single component of the magnetic field: $B_x = B_0 \tanh(z/L)$, where B_0 is the magnetic field amplitude, L is CS thickness. Corresponding single component of the current density $j_y = (cB_0/4\pi L)\cosh^{-2}(z/L)$ is supported by diamagnetic drift of the entire populations of ions and electrons. Thus, the profile of current density coincides with the profile of plasma density, while the drift velocity and plasma temperature are constant across CS. Magnetic field pressure in such CS is balanced (along the normal) by variation of perpendicular plasma thermal pressure $p_\perp(z)$: $8\pi p_\perp(z) + B_x^2(z) = \text{const}$.

Although Harris (1962) CS model is very popular and easy for applications, it cannot describe the realistic magnetotail CS due to absence of the B_z magnetic field component. This

component, in a natural configuration connects magnetic field lines in southern and northern magnetotail lobes through the neutral plane $z = 0$ (at least for the near-Earth region, $X > -30\ R_E$). Even small, but finite B_z component destroys the self-consistency of Harris (1962) model, since the tension of magnetic field lines $\sim j_y B_z$ remains unbalanced. This force can be compensated by the gradients of a plasma pressure $\partial p/\partial x$ in 2D models. Such a scenario is realized in several 2D CS models with isotropic pressure tensor (Schindler 1972; Kan 1973; Schindler and Birn 2002; Yoon and Lui 2005; Vasko et al. 2013). In case of 2D models with isotropic pressure the L_x-scale of system inhomogeneity along the tail is coupled to the CS thickness L_z and amplitudes of magnetic field components: $L_x = L_z B_0/2B_z$ (Burkhart and Chen 1993).

The alternative approach to compensation of $\sim j_y B_z$ force takes into account the anisotropy of plasma pressure (Rich et al. 1972; Francfort and Pellat 1976; Cowley and Pellat 1979), which can be generated by transient nonadiabatic ions (Speiser 1965, 1967). This approach allows to construct a 1D CS model with a finite B_z component and ion beams at system edges (see, e.g., Sitnov et al. 2006 and review by Zelenyi et al. 2011). In 1D models L_x is formally infinite (much larger than the estimate made above for 2D models). The main current in such 1D models is carried by transient hot ions. The bulk velocity of such ions is comparable with their thermal velocity and, as a result, rather small ion population can support almost the entire cross tail current required for the magnetotail field reversal Eastwood (1972, 1974).

Modern models are capable to describe almost all details of CS observations obtained thus far (Sitnov et al. 2006; Artemyev et al. 2008; Zhou et al. 2009). To fit the vertical (along the normal) profile of current density, we can pick up any model with a necessary number of free parameters (Yoon and Lui 2004; Birn et al. 2004; Zelenyi et al. 2004; Artemyev et al. 2009). Moreover, even simple Harris (1962) CS model can be fitted to observations after some modifications (Petrukovich et al. 2011). The primary difference between CS models is in their configurations along the magnetotail (e.g., the principal choice is between 2D isotropic and 1D anisotropic models). Another way is to compare the kinetic structure of plasma distributions in observed CSs and the one predicted by different models (see details in Artemyev and Zelenyi 2013).

3 Dataset and Methods of Processing of Multispacecraft Measurements

To investigate CS structure we use measurements of multispacecraft Cluster mission (Escoubet et al. 2001). Magnetic fields are measured by FGM experiment (Balogh et al. 2001), electric fields are measured by EFW experiment (Gustafsson et al. 2001), electron distribution functions are measured by PEACE experiment (Johnstone et al. 1997), while ion velocity distributions are measured by CIS/HIA/CODIF experiment (Rème et al. 2001). The time resolution of measurements of electron and ion distribution functions is 4–16 seconds (1–4 spacecraft spins). We use electric and magnetic field data with time resolution corresponding to one point per 4s or five points per second. The main statistics of CS crossings is based on the first four years (2001–2004) of measurements, when distances between spacecraft were of the order **of ion scale**: 1000 km, 3000 km, 300 km, 600 km. During this period Cluster crossed magnetotail CS at 14–20 R_E from Earth. The data collected in later years (2005–2009) with the larger distances between spacecraft are used to investigate the magnetic field gradients along the tail.

The main advantage of multispacecraft missions is a possibility of simultaneous measurements at four positions. Using magnetic field data at four points (properly spaced, e.g., in a

form of tetrahedron) one can estimate the magnetic field gradient. Corresponding assumptions and estimations of errors are described in details in several papers (Dunlop et al. 2002; Runov et al. 2005b; Paschmann and Schwartz 2000). Gradient of B_x component can be used to determine the direction of normal to CS for typical magnetotail configuration. Gradients of all three magnetic field components give an estimate of the curl of magnetic field curl $\mathbf{B}$, i.e. the electric currents. This method is called "curlometer" technique. For the majority of observed CSs the main component of curl $\mathbf{B}$ is dB_x/dz.

The alternative method to determine the normal direction and the magnetic field gradient is the timing technique. In this case, time delays between observations of the same magnetic field features at different spacecraft provide the estimates of the direction and velocity of CS motion along the normal. This velocity is later used to recalculate the time delays to spatial scale.

To unify the consideration of CS, the local coordinate system $(\mathbf{l}, \mathbf{m}, \mathbf{n})$ could be introduced. For a model 1D current sheet it is in fact cartesian, the gradient of B_l component of magnetic field is supported by the current density j_m. For real data obtained vectors are not exactly orthogonal and a certain procedure is necessary (Runov et al. 2005b). $\mathbf{l}$ vector is defined as a direction of a maximum variation of magnetic field. The current density vector $\mathbf{j}$ is used to determine the vector $\mathbf{m} = \mathbf{j}/j - (\mathbf{lj})/j$. The normal vector completes the system to right-handed one: $\mathbf{n} = [\mathbf{l} \times \mathbf{m}]$.

The profiles across the current sheet (along the normal) are taken during episodes of fast relative motion of a spacecraft and current sheet (usually within 10 min for a thin sheet) and require assumption of stationarity of CS. The combination of current density j_m profiles and magnetic field B_l as a nonlinear coordinate across CS allows us to restore the spatial gradient of any plasma parameter A measured by a single spacecraft (Zelenyi et al. 2010; Artemyev and Zelenyi 2013): $dA/dz = (4\pi/c)\, j_m (dA/dB_l)$ (e.g. A can be an ion or electron temperature, or plasma pressure).

The determination of CS thickness L (scale along the normal) requires additional assumptions, because L definition depends on the particular profile of j_m. In this review we estimate $L = cB_0/4\pi j_0$, B_0 and j_0 are the maximal value of magnetic field and current density. The determination of B_0 is not straightforward, because B_0 (maximal field in the thin current sheet) can differ substantially from the magnetic field B_{ext} at lobes. In general case the magnetic field B_{ext} can be readily estimated using the vertical pressure balance:

$$B_{ext}^2/8\pi = B_l^2/8\pi + P_{th}$$

where P_{th} is a plasma (ions and electrons) thermal pressure. In the next section we describe possible approaches for the determination of B_0.

4 Embedding of CS

To illustrate the main properties of CSs observed by Cluster in the Earth magnetotail we use the figure published in one of the first statistical papers by Runov et al. (2005a, 2006). Figure 1 demonstrates the profiles of current and plasma densities across the sheet (as a function of B_l magnetic field component normalized on the lobe field B_{ext}). In contrast to Harris (1962) model, in which profiles of current density and plasma density coincide exactly, in observed CS both these profiles are very different: the current density profile is much narrower than the plasma density one. The average profile of plasma temperature is similar to the density profile. Thus, the current sheet is localized deeply inside the plasma density profile and such a configuration is called embedded sheet.

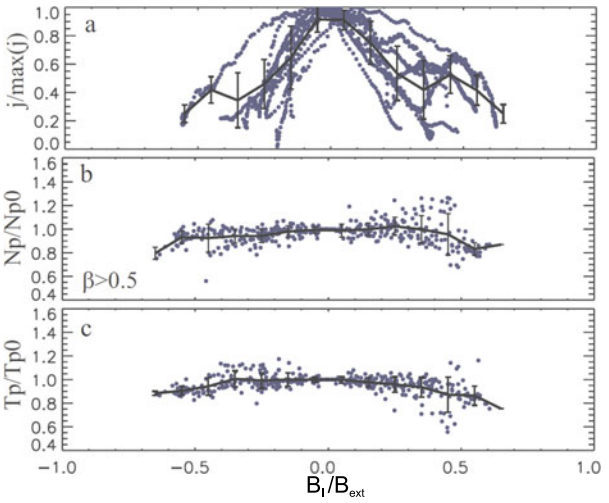

Fig. 1 Profiles of current density (**a**), plasma density (**b**) and temperature (**c**) across the CS. The plasma and current densities are normalized to their value at the neutral sheet ($B_l = 0$). The profiles averaged over the statistics are shown by solid curves. Figure is adopted from Runov et al. (2006)

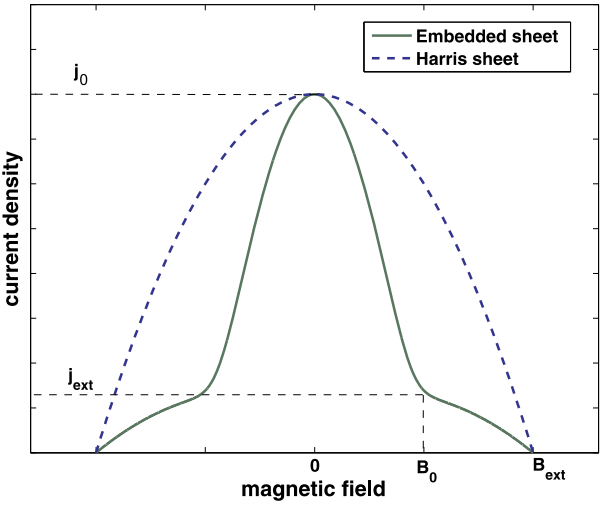

Fig. 2 Schematic view of current density profile in the embedded CS (*green curve*) and in simple CS described by Harris (1962) model. Figure is adopted from Petrukovich et al. (2011)

In absence of CS embedding we can characterize the CS configuration by two parameters: magnetic field amplitude at lobes B_{ext} and CS thickness L_{ext} (or maximal current density $j_0 = cB_{ext}/4\pi L_{ext}$). The current density amplitude j_0 can be derived from four-point measurements of magnetic field. B_{ext} can be estimated using the vertical pressure balance.

To describe the embedded CS one should introduce at least two additional parameters (Fig. 2): B_0 is magnetic field amplitude at the boundary of thin embedded CS and j_{ext} is the current density amplitude at the boundary of thin embedded CS. In the most of cases two parameters j_{ext} and j_0 cannot be estimated for the same CS, because Cluster spacecraft can probe reliably only one scale corresponding to the distance between spacecraft, while we often have $j_{ext} \ll j_0$ and, as a result, $L_{ext} \gg L = cB_0/4\pi j_0$. To measure weaker magnetic field gradients related to j_{ext} one needs larger spacecraft separation. Thus, only B_0 can be considered as a practical parameter characterizing embedded CS.

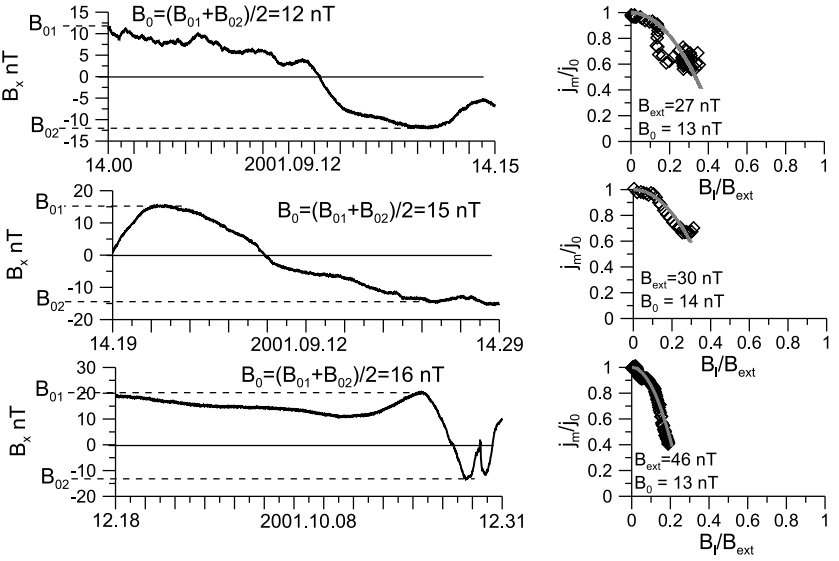

Fig. 3 Three examples of B_0 determination. On the *left panels* B_0 is estimated as the average of magnetic fields observed at the CS boundaries, $B_0 = (B_{01} + B_{02})/2$. On the *right panels* B_0 is estimated using the profile of the current density (see text for details). Figure is adopted from Artemyev et al. (2010)

Although, magnetic field measurements are reliable nowadays, the determination of B_0 is not a straightforward task. The main problem is the determination of the boundary of thin embedded CS. This boundary can be accurately defined only in case of substantial difference between thicknesses of embedded and enveloping CSs. Artemyev et al. (2010) introduced two approaches to the B_0 determination. The first one assumes that B_l variation is due to motion of the CS relative to motion of the spacecraft. Then B_0 can be defined as a B_l value measured at the moment when variation rate of B_l is substantially reduced, when the spacecraft escapes the thin CS with strong electric current (Fig. 3, left panels). The second approach approximates current density profile by a function of B_l field, $j_m = j_0(1 - sB_l^2)$, with s as a free parameter, so that $B_0 \approx s^{-1/2}$ (Fig. 3, right panels). The accuracy of both methods is about 10–20 %. Thus, it is more reliable to analyze the statistics of B_0 values rather than B_0 for individual crossings.

The statistics of CS crossings by Cluster spacecraft (42 examples, see Artemyev et al. 2010) allows us to consider the distribution of B_0/B_{ext} ratio. For the most of cases B_0/B_{ext} is about 0.3–0.5 with the average value ≈ 0.4 (Fig. 4). The ratio of the current densities measured in the center and at the boundary of thin CS (where $0.9 < |B_l/B_0| < 1$) is about $\sim$5. The variation of plasma density across thin CS does not exceed 25 % in agreement with an estimate given by the pressure balance $(B_0/B_{ext})^2 \sim 0.16$.

The strong variation of the current density across CS without corresponding variation of the plasma density suggests that the main current in this thin embedded CS is carried by a relatively small (10–15 %) ion population with a large bulk velocity. An estimate of this velocity can be obtained as a ratio of measured (curlometer) current density and a variation of the plasma density. Such estimate gives a bulk velocity (along the direction of the electric current) about the thermal ion velocity (Artemyev et al. 2010). Presence of such ion population is predicted by the models with transient ions (Ashour-Abdalla et al. 1991, 1993; Burkhart et al. 1992a; Kropotkin et al. 1997; Sitnov et al.

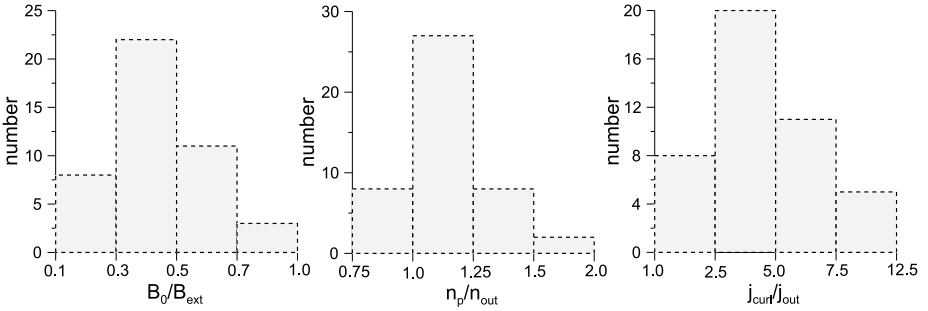

Fig. 4 Histograms of ratio B_0/B_{ext}, ratios of plasma and current densities at CS center ($B_l = 0$) and at CS boundaries ($0.9 < |B_l/B_0| < 1$). Figure is adopted from Artemyev et al. (2010)

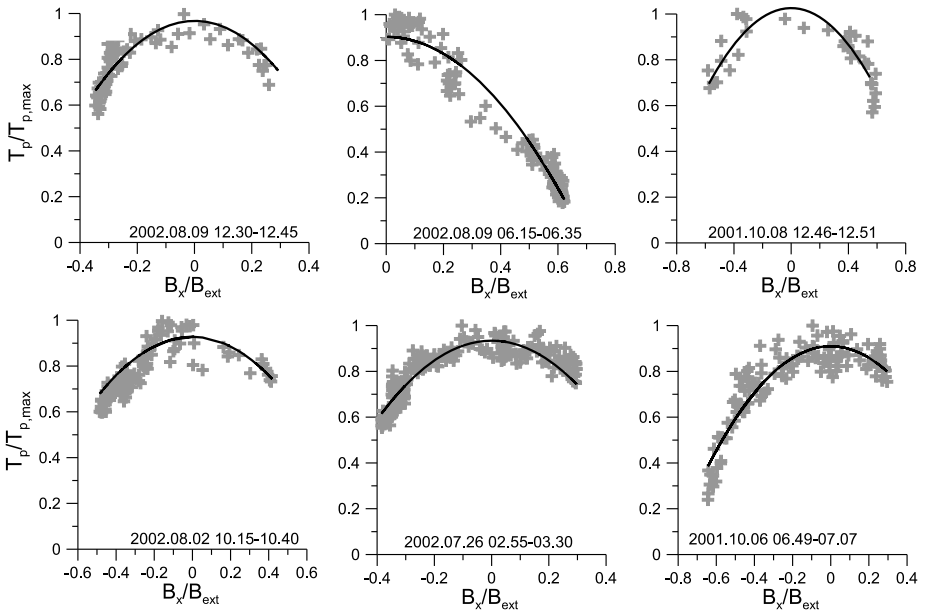

Fig. 5 Several examples of proton temperature distribution across the CS. Temperature is normalized on its value at CS central region. Figure is adopted from Artemyev et al. (2011a)

2000; Zelenyi et al. 2000). Figure 1c and previous investigations (Hoshino et al. 1996; Runov et al. 2006) have shown that proton temperature also vary substantially across the tail. A detailed Cluster analysis (Fig. 5) results in an approximation by a simple function $T_p = T_{p,\max}(1 - \alpha_T(B/B_{ext})^2)$, $\alpha_T \approx 0.8$. If this temperature increase in the CS center is also due to current-carrying ions, their temperature is three-five times larger than the background temperature (Artemyev et al. 2011a).

A similar to Fig. 5 variation is found for the electron temperature (see Zelenyi et al. 2010; Artemyev et al. 2012). These variations of ion (proton) and electron temperatures are often more significant than the variation of the plasma density. The scale of T_p variation can be estimated as $L_T \sim |d \ln T_p/dz|^{-1}_{B_x \approx 0} \approx (B_{ext}/\alpha_T B_0)L \approx (2-10)L$ (L is the CS thickness).

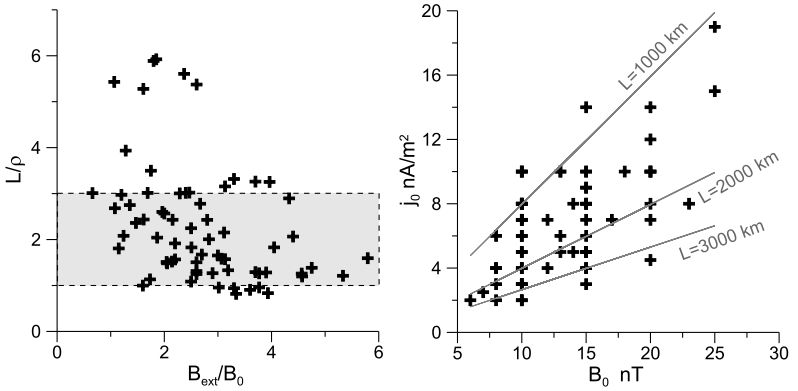

Fig. 6 *Left panel* shows the dependence of ratio L/ρ on B_{ext}/B_0 value (both CS thickness and proton Larmor radius are calculated with B_0 field). *Right panel* shows the current density amplitude j_0 versus B_0 field. *Three lines* correspond to characteristic CS thicknesses

Finally one can test the relation between the CS thickness and typical plasma spatial scales (Larmor radius ρ and/or ion inertial length). For the most of CSs it was shown that the ratio L_{ext}/ρ_{ext} (where proton Larmor radius ρ_{ext} and L_{ext} are calculated with B_{ext}) varies in a wide range with the mean value $\sim$10 (Runov et al. 2005a, 2006). However, if we recalculate the Larmor radius and CS thickness, using the magnetic field B_0 at the boundary of thin embedded CS this ratio should substantially decrease $L/\rho = (L_{ext}/\rho_{ext})(B_0/B_{ext})^2 \sim 0.2(L_{ext}/\rho_{ext})$. To verify this estimate we plot L/ρ as a function of B_{ext}/B_0 for statistics of 72 CS crossings (Artemyev et al. 2011a) in Fig. 6. For almost all CSs L/ρ is within the range [3, 1]. Thus, for observed CSs we can use the proton Larmor radius calculated in B_0 field as a very good approximation for CS thickness. In such a case the current density amplitude j_0 should grow with B_0. Indeed, this growth can be found (right panel in Fig. 6).

As ρ also depends on the proton temperature T_p, the CS thickness should increase with T_p. We select two groups of CSs with different temperatures ($T_p < 4$ keV and $T_p > 8$ keV) and normalize CS thicknesses on the Larmor radius calculated for $T_p = 3$ keV. Resulting current density profiles are in Fig. 7. One can clearly see the increase of CS thickness with T_p.

Another test of relation $L/\rho \approx$ const can be done using the variable content of oxygen ions O^+ (up to 50 % of total plasma density). In CSs with larger oxygen content the corresponding thickness should be larger because for the same temperature the Larmor radius of oxygen ion is four times larger than the proton Larmor radius. We select three groups of CSs with different populations of oxygen ions and normalize CS thicknesses on the proton Larmor radius calculated with the measured temperature (Fig. 8). The increase of oxygen content clearly results in the increase of CS thickness.

Although, Fig. 6 shows that for the majority of observed CSs the thickness is about 1–3 proton Larmor radii (or 1000–3000 km), there is one specific class of CSs with smaller thickness. These CSs are observed in the vicinity of X-lines and often have current density amplitudes higher than 30 nA/m^2 (Nakamura et al. 2006, 2008). Corresponding thickness of such intense CSs is about ion inertial length $d_i \approx \rho(B_0/B_{ext})$ and is smaller than the proton Larmor radius. However, it is still much larger than the electron Larmor radius, $L/\rho_e \in [5, 30]$ (Artemyev et al. 2013a). The example of such intense CS is shown in Fig. 9. Comparison of the curlometer current density and electron moments shows that almost all

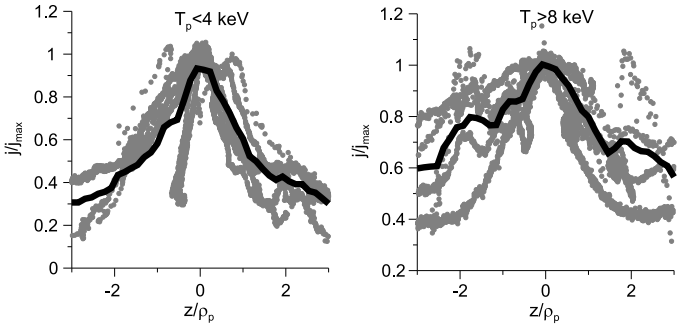

Fig. 7 Profiles of normalized current density for two groups of CSs with different proton temperatures. *Black curves* show the average profile. Figure is adopted from Zelenyi et al. (2011)

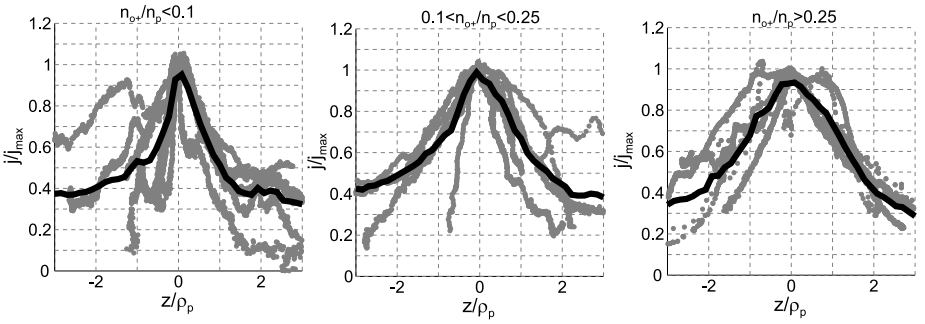

Fig. 8 Profiles of normalized current density across the CS for three groups of CSs with different densities of oxygen ions with respect to total plasma density. *Black curves* show the average profile. Figure is adopted from Zelenyi et al. (2011)

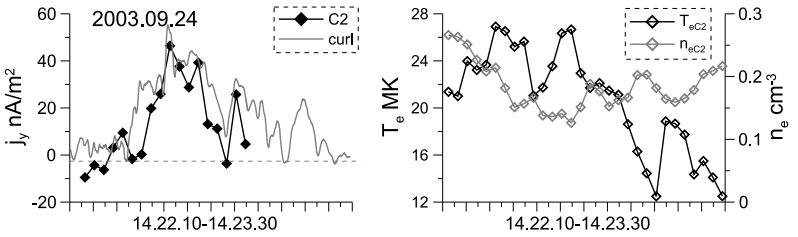

Fig. 9 *Right panel* shows the profile of current density in the intense CS: *grey color* is for current density calculated by curlometer technique, while *black color* is for electron current density measured by PEACE experiment onboard Cluster 2 spacecraft. *Left panel* shows profiles of electron temperature and electron density across CS. Figure is adopted from Artemyev et al. (2013a)

observed current density is due to the electron current (for this CS $L/\rho_e \approx 12$). There is almost no variation of electron density (and plasma density as well) across the sheet, while the electron temperature has a significant maximum in center of CS. Due to small CS thickness the ion temperature does not vary across the sheet and the pressure balance is supported by specific configuration of parallel currents creating a local maximum of B_m field in the central region of CS (see details in Artemyev et al. 2013a) (these curves are not shown here).

Investigations of such intense thin CS is possible only for one season of Cluster observations when spacecraft separation was small enough (2003). However, even for this season the time resolution of measurements of plasma parameters does not allow us to study well an internal structure of these CSs. Thus, the detailed investigation of these important class of CS could be performed only in future missions (like MMS).

5 Ion Kinetics

Vertical profiles of plasma and current densities indicate that the main cross-tail current should be carried by a relatively small part of ion population contributing only about ∼10–15 % to the total plasma density with large bulk velocity along the dawn-dusk direction. Thus, it is interesting to reveal its velocity distribution. However, only in a few cases the observed ion current density is close to the value of current density estimated using the curlometer (magnetic field gradient) technique (see next section for more details). Thus, to study ion kinetics in embedded CSs we identify several crossings having strong ion currents (Artemyev et al. 2010). One example is shown in Fig. 10. There is a strong increase of ion bulk velocity u_y up to 100 km/s in the central region of CS, while the plasma density varies very weakly.

To reveal reliably the current-carrying ion population we divide the whole time interval of CS crossing into five subintervals (see numbers in Fig. 10). For each subinterval we calculate the average ion distribution $f(v_x, v_y)$. Then, we calculate the differences $\Delta f_i(v_x, v_y) = f_i(v_x, v_y) - f_0(v_x, v_y)$ for $i = 1..4$ (interval "0" is out of the current sheet). Distributions $\Delta f_i(v_x, v_y)$ should contain the ion population which is present in the center and absent at the CS boundary, and thus is mainly responsible for the support of the transverse current. Right panels of Fig. 10 demonstrate that positive $\Delta f_i(v_x, v_y)$ (grey color) corresponds to an ion population mostly located in the $v_y > 0$ domain. Distribution of this population in velocity space has a local maximum at $v_y > 0$ (there are almost no particles for $v_y < 0$) and, thus, can be considered as a beam. However, it should be mentioned that the same distribution is often called bean distribution due to the half-ring shape in (v_x, v_y) plane. Its shape resembles in

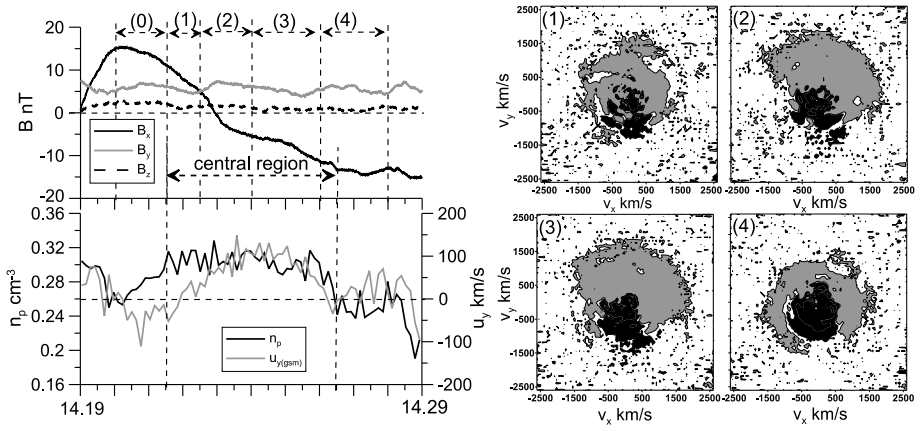

Fig. 10 CS crossing at 12 September 2001. *Left panels* show profiles of magnetic field, plasma density and ion bulk velocity. *Right panels* show $\Delta f_i(v_x, v_y)$ distributions. *Grey color* corresponds to $\Delta f_i > 0$ and *black color* to $\Delta f_i < 0$ (see text for details). Figure is adopted from Artemyev et al. (2010)

many aspects the theoretical distribution of transient ions (see corresponding comparison and discussion in Artemyev and Zelenyi 2013). Artemyev et al. (2010) demonstrated that all observed (measured by the curlometer technique) current density can be almost fully supported by these ions if their density is only about 10–15 % of the total plasma density which is in agreement with the measured variation of the plasma density (see Fig. 4).

An additional interesting question concerns a possible contribution of high-energy ions (energy larger than 35 keV) to the cross-tail current. The Cluster CIS/CODIF experiment (Rème et al. 2001) measures ion velocity distributions for energies below 35 keV, while for high-energy ions one should consider data obtained by the RAPID experiment (Wilken et al. 2001). However, the accuracy of the ion flow data obtained from high-energy ion measurement is not sufficient for estimations of the corresponding current density. Nonetheless, by extrapolating the velocity distribution profile to high energy range gives an upper limit of a possible current density carried by ions with energies above 35 keV. For several CSs with relatively high ion temperature (7–9 keV) Artemyev et al. (2009) estimated this upper limit to be less than 30 % of the total ion current. However, for the total plasma pressure the contribution of high energy ions can be larger (see discussion in Runov et al. 2006).

6 Current Carriers and Sources of Electron Currents

Accurate and regular measurements of electron velocity distribution by Cluster spacecraft allow for the first time to perform a comprehensive statistical investigation of electron parameters in CS. We compare electron currents with currents estimated by curlometer technique. First of all, it is important to demonstrate that the sum of ion and electron currents is equivalent to curlometer current density. Figure 11 shows two examples of CSs, in which the sum of ion and electron currents approximate curlometer data quite well (see details in Artemyev et al. 2009).

To analyze the relation between particle currents and curlometer data over a broader statistics we consider averaged values of currents calculated for $|B_l| < 5$ nT. For each crossing we identify three values: average ion current j_i, average electron current j_e, and average curlometer current j_{curl}. Comparison of these three values shows (see Fig. 12 and publications (Asano et al. 2003; Israelevich et al. 2008; Artemyev et al. 2009)): 1. for the most of observed CSs j_i is significantly smaller than j_{curl}, while the sum $j_i + j_e$ describes j_{curl} on average quite well; 2. there are CSs with negative and positive j_i, while j_e is almost always positive; 3. for some CSs the sum $j_i + j_e$ significantly differs from j_{curl}. The last effect can be explained in several ways. First of all, there could be a technical problem related to the

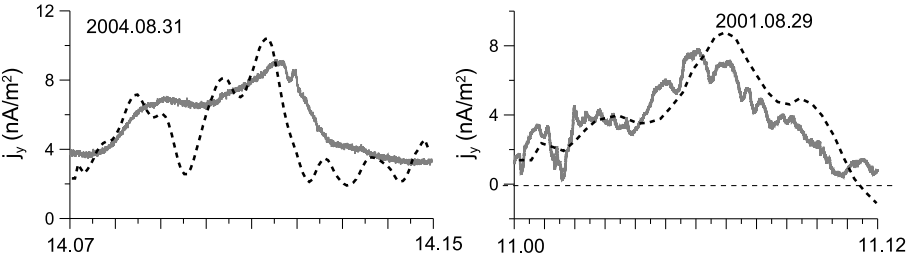

Fig. 11 Two CS crossings: *grey solid curve* shows curlometer estimates of the current density, while *dashed black curve* shows the smoothed profiles of the sum of electron and ion currents. Figure is adopted from Artemyev et al. (2009)

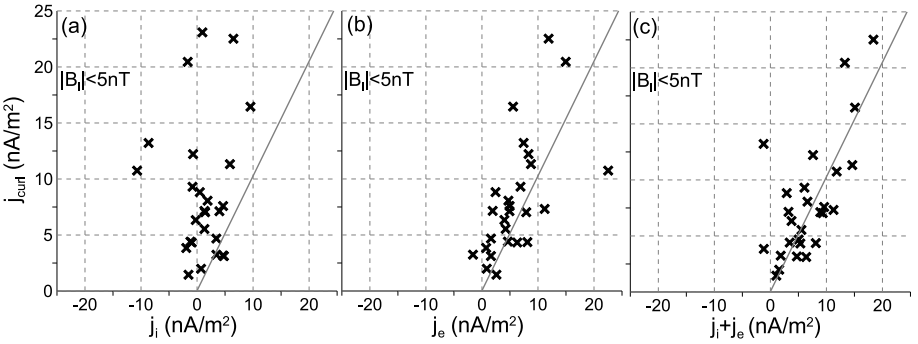

Fig. 12 Comparison of curlometer estimate of the current density j_{curl} with (**a**) ion current density j_i, (**b**) electron current density j_e, (**c**) amplitudes of sum of particle currents $j_i + j_e$. Figure is adopted from Artemyev et al. (2009)

reliability of the measurements of particle currents. These measurements are performed with the time resolution 4–16 s. For some fast crossings of CSs this resolution can be insufficient for reliable determination of maximal current. Second, the finite energy range of particle measurements can result in underestimation of particle currents. Third, one cannot exclude the possibility of fast variations of particle currents. For example, Asano et al. (2004a, 2003) demonstrated the presence of fast substantial variations of electron currents in CSs. These variations can be considered as a manifestation of natural small-scale electron substructures in CS. However, detailed analysis of this problem requires more accurate measurements of particle velocity distributions, e.g. in a future MMS project (Burch et al. 2014).

To explain surprisingly large contribution of electrons to the total cross-tail current we estimate three main components of the electron current density: diamagnetic drift current, curvature drift current, and cross-field drift current. The electron diamagnetic drift current is proportional to the ratio of particle temperatures $T_e/(T_e + T_i)$ (Artemyev and Zelenyi 2013). Cluster statistics gives $T_i/T_e \sim 3.5$–5 (Artemyev et al. 2011b), and electron diamagnetic effects can be responsible only for 10–20 % of the total electric current. Amplitude of electron drift curvature current density is about $j_{curl}(T_{e\|}/T_{e\perp} - 1)4\pi T_{e\perp}/B_z^2$ (Artemyev and Zelenyi 2013). Temperature anisotropy of electron population in CSs is about $T_{e\|}/T_{e\perp} \sim 1.1$–1.2 (Artemyev et al. 2012) and for some CSs the curvature currents indeed can be comparable with the total curlometer current density. However, for the most of CSs the curvature drift current gives less than 50 % of j_{curl} (Zelenyi et al. 2010). Thus, the remaining 50 % should be provided by electron cross-field drift $v_{E\times B} = c\mathbf{E} \times \mathbf{B}/B^2$. This drift does not produce any total current but reduces ion contribution and increases the electron one (Artemyev et al. 2011a). Estimate of $v_{E\times B}$ gives ~ -40 km/s for the abundant statistics of observed CSs (Zelenyi et al. 2010).

For the classical CS configuration $v_{E\times B} = c(E_z B_x - E_x B_z)/B^2 \approx cE_x/B_z$ in the CS central region where $B_x \sim 0$. To get $v_{E\times B} \sim -40$ km/s one needs an electric field $E_x \sim 0.15$ mV/m. So small electric field cannot be measured in the magnetotail and was never broadly discussed. However, positive E_x was obtained in laboratory modelling of the magnetotail CS (Minami et al. 1993). The model of E_x field as a part of ambipolar (polarization) electrostatic field can be developed for weakly 2D CSs (Zelenyi et al. 2010). Estimates based on Cluster observations show that the drift $v_{E\times B}$ can indeed significantly reduce current of transient ions or even result in negative values of observed ion current density (Artemyev et al. 2011a; Artemyev and Zelenyi 2013). Taking into account the role of this *hidden* elec-

tric field (which, by itself, does not produce any cross-tail current) enables to explain many paradoxical features of current observations in the magnetotail (see Fig. 12).

7 Tilted Current Sheets

In the classical configuration of the Earth magnetotail the current sheet is horizontal: the main gradient of magnetic field B_l is directed along the north-south direction (Z-axis), the main component of the normal vector **n** in the GSM is n_z. The current is in equatorial plane, the main component of vector **m** is m_y. Cluster spacecraft discovered a new type of CSs with vector **n** directed almost along the dawn-dusk direction and an electric current flowing almost along the Z-axis (Zhang et al. 2002; Petrukovich et al. 2003; Sergeev et al. 2006). We call CSs with $n_y > 0.85$ strongly-tilted—the angle between vector **n** and the Y-axis is smaller than 30°. Formation of strongly-tilted CSs and their structure are considered also in several later publications (Petrukovich et al. 2006, 2008; Rong et al. 2010; Vasko et al. 2014a).

One example of the observation of a strongly-tilted CS is presented in Fig. 13. This example demonstrates the main properties of the strongly-tilted CSs in the statistical study by Vasko et al. (2014a): The magnetic field has a significant B_m (B_z in the GSM) component, on average B_m is about ∼7 nT (see also Petrukovich et al. 2003), $B_m/B_0 \sim 0.45$. B_n component (B_y in the GSM) is much smaller than B_m, on average B_n is about ∼1.5 nT, $B_n/B_m \sim 0.35$. Almost all current is along the Z-axis so that a significant portion of this current is field-aligned with respect to the magnetic field, $j_\parallel/j_\perp \sim 2.1$. Almost all current is carried by electrons (Vasko et al. 2014a).

Strongly-tilted CSs represent locally 1D structures with the magnetic field configuration resembling the horizontal CSs with a strong shear magnetic field B_m (or B_z in the GSM system) (Petrukovich et al. 2007; Nakamura et al. 2008; Shen et al. 2008; Rong et al. 2012). The presence of a strong shear component drastically changes charged

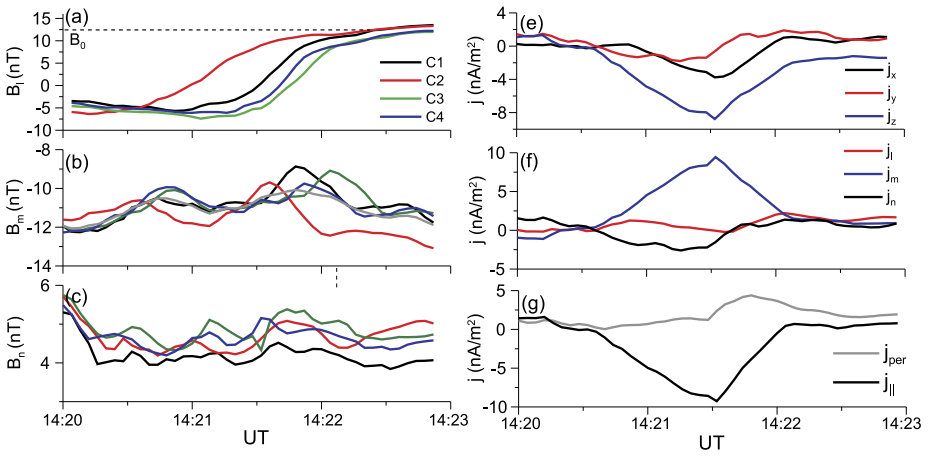

Fig. 13 An example of a strongly-tilted CS crossed by Cluster on 7 September 2004: (**a**), (**b**), (**c**) the magnetic field observed by four Cluster spacecraft in the local coordinate system; (**e**), (**f**) the current density determined by the curlometer technique in the GSM system and in the local coordinate system, respectively; (**g**) the components of the curlometer current density parallel and perpendicular to the magnetic field. Figure is adopted from Vasko et al. (2014a)

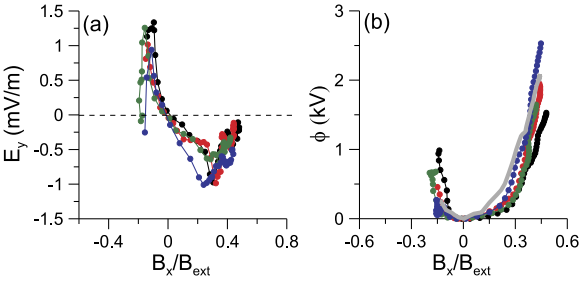

Fig. 14 Profiles of the polarization electric field (**a**) and the corresponding scalar potential (**b**) across the CS for the event presented in Fig. 13. *Grey curve* presents the theoretical profile $\phi = T_p(B_x/B_{ext})^2$. Figure is adopted from Vasko et al. (2014a)

particle dynamics (Büchner and Zelenyi 1989; Artemyev et al. 2013a). The particle dynamics is determined by the adiabaticity parameter κ that is the ratio of the field line curvature to the particle Larmor radius at the neutral sheet (where $B_l \approx 0$). For horizontal CSs with a small shear component the curvature radius in the neutral sheet is about $(B_n/B_0)L \sim L/10 \sim$ 100–200 km, while for strongly-tilted CSs (with large shear) it is about $(B_n/B_0)(1 + (B_m/B_n)^2)L \sim 1.5L \sim 3000$ km. Thus, in horizontal CSs the curvature radius is smaller than the ion Larmor radius (Runov et al. 2006) and the adiabaticity parameter κ_p is generally smaller than 0.5. For tilted CS the curvature radius is larger than ion Larmor radius and generally $\kappa_p > 0.5$ (Vasko et al. 2014a). As a result in horizontal CSs the ion dynamics is quasi-adiabatic (Zelenyi et al. 2013), while in strongly-titled CSs the ion dynamics is likely stochastic. In both horizontal and strongly-titled CSs the curvature radius is significantly larger than electron Larmor radius so that $\kappa_e > 3$ and hence electrons are magnetized.

Strongly-tilted CSs provide one additional opportunity for investigation of general CS structure. The decoupling of motions of chaotic (or quasi-adiabatic) ions and magnetized electrons should result in generation of (polarization) electric fields if CSs are sufficiently thin (Schindler et al. 2012). This field has two components—E_n and E_l (i.e. E_z and E_x in horizontal CSs) (Zelenyi et al. 2004; Birn et al. 2004). As has been mentioned in the previous section, E_x component plays an important role in the redistribution of intensities of ion and electron currents and is coupled with the E_z component (Schindler and Birn 2002; Zelenyi et al. 2010). However, the configuration of the probe measurement (perpendicular to spacecraft rotation axis) at Cluster spacecraft does not permit to measure $E_n \approx E_z$ in horizontal CSs. In contrast, in strongly tilted CSs $E_n \approx E_y$ can be already reliably measured. E_y is the sum of convection and polarization electric fields. The former one corresponds to the large-scale earthward plasma convection and is about 0.1–0.3 mV/m (Kennel 1973; Angelopoulos et al. 1993). This field does not vanish at the neutral sheet, while the polarization field equals zero therein. Thus, one can determine and subtract convection field from the observed electric field E_n.

Vasko et al. (2014a) have determined the profiles of the polarization electric field E_y for statistics of strongly-tilted CSs (Fig. 14(a)): E_y has an asymmetrical profile across the CS ($E_y B_x > 0$) and the amplitude of about 0.5–1 mV/m. Integration of E_y across the CS gives the profile of the scalar potential ϕ (Fig. 14(b)). For statistics of tilted CS the amplitude of ϕ is about few kV, while ϕ-profile has a minimum at the neutral plane and can be well described by following equation in accordance with the model expectations (Vasko et al. 2014a)

$$\phi = T_p \frac{B_x^2}{B_{ext}^2}$$

where T_p is ion temperature.

8 Current Sheet Dynamics During Substorm Growth Phase

Dynamics of the magnetotail current sheet during growth phase of geomagnetic substorm is of particular interest (Petrukovich et al. 2007, 2013; Snekvik et al. 2012; Davey et al. 2012) because CSs are assumed to serve as accumulators of magnetic field energy stored in the magnetotail. Being driven by the global magnetospheric convection the tail plasma sheet thins and the entire magnetic configuration stretches from more dipolar to more tail-like geometry. As a result an intense CS with a thickness of the order of several thousand kilometers forms in the plasma sheet. Prior to Cluster mission this process was characterized mainly by the decrease of B_z magnetic field. Cluster provided regular measurements of the cross-tail current density and, in some cases, of horizontal magnetic gradient $\partial B_z/\partial x$. It should be noted, however, that the task of prolonged (tens of minutes) monitoring of CS is in a certain contradiction with the basic method of its study (using the fast crossings as described in previous sections). Thus, some sheet parameters are determined less reliably (in particular, B_0).

There were 39 Cluster CS observations during growth phase in 2001, 2002, 2004 at distances 17–20 R_E downtail (Petrukovich et al. 2007). An example is in Fig. 15. The key moment is the determination of an instant of substorm onset. Properties of CS directly before an onset may provide important information on the development of an expected magnetotail instability. In this case the onset was defined as the beginning of tailward flow (negative V_x) at 13:01 UT.

Before the onset the classical isolated growth phase was observed for about 40 min. During the growth phase the total magnetic field in the tail lobes B_{ext} increased from 29 to 32 nT (calculated using the full pressure), denoting the accumulation of open magnetic flux. The current density increased from 2 to 8 nA/m^2, but the maximum current density of 15 nA/m^2 was registered just after onset. B_z decreased from 5 to 2 nT. The small up-and-down CS oscillations allowed to recover the current density profile and estimate the

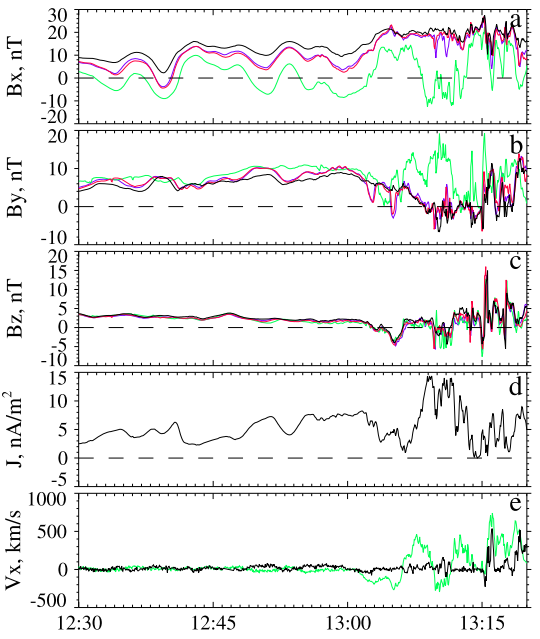

Fig. 15 Current sheet, observed September 12, 2001: (**a**)–(**c**) magnetic field; (**d**) current density, (**e**) proton bulk velocity V_x. *Colors* denote the satellite (C1)–(C4), respectively: *black*, *red*, *green*, *blue*. Figure is adopted from Petrukovich et al. (2009)

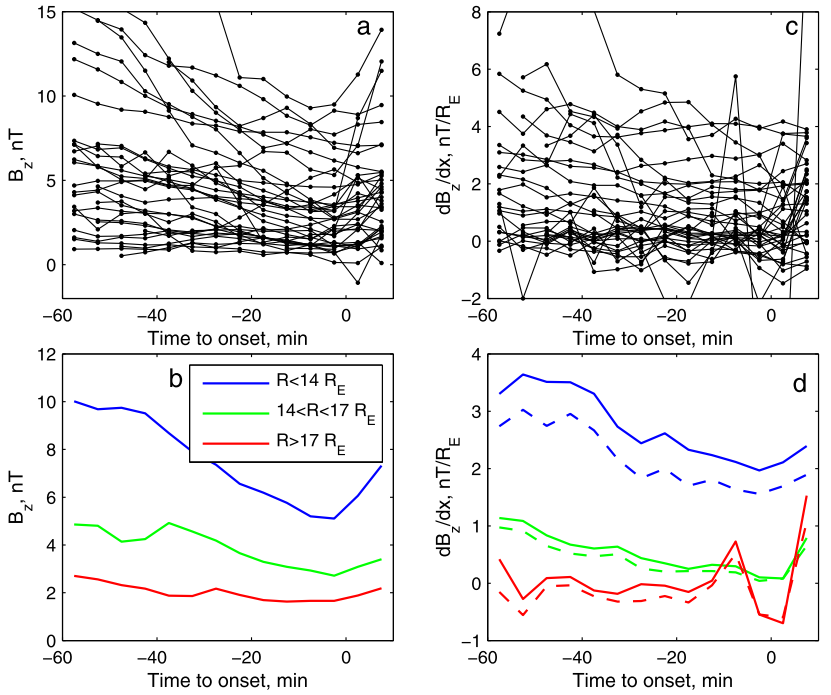

Fig. 16 Evolution of B_z (**a**) and $\partial B_z/\partial x$ (**c**) with respect to onset time for 59 events with a 5 minute averaging. Averaged profiles of B_z (**b**) and $\partial B_z/\partial x$ (**d**) in the three ranges of downtail distances. At the panel (d) *solid lines* correspond to the gradient $\partial B_z/\partial x$, *dashed lines*—to $\partial B_z/\partial r$. Figure is adopted from Petrukovich et al. (2013)

increase of B_0/B_{ext} from 0.3 to 0.5. The estimate of sheet thickness gives several thousand km and could not be accurate because of the uncertainty in B_0. These parameters are close to average for the whole dataset of 39 crossings.

Cluster orbit after 2005 allowed to probe also the near-Earth magnetotail (up to 9 R_E downtail), where one expects a significant influence of two-dimensionality on the formation of the current sheet. For the period 2005–2009 59 observations of growth phase have been identified, in which small longitudinal gradients of magnetic field $\partial B_z/\partial x$ were measured. These measurements become possible due to substantially increased spacecraft separation after 2005 (Petrukovich et al. 2013).

General statistics of gradient $\partial B_z/\partial x$ and B_z for three ranges of downtail distances is shown in Fig. 16. At a distance more than 17 R_E a negligible gradient was registered (fluctuating around zero, but the error in our data set is not less than 0.5 nT/R_E). B_z average also changes a little and is about 2 nT. This is the zone of elongated almost one-dimensional sheet. Sharp changes in the gradient near onset are produced by the earthward motion of dipolarization fronts and thus essentially represent an unavoidable uncertainty of onset time definition. Near the Earth at a distance less than 14 R_E there is a clear decrease of the average gradient from 3–4 to 2 nT/R_E, and B_z from 10 to 6 nT. This is the zone where the effects of second dimension play an essential role. At the range of distances 14–17 R_E properties of magnetic field are intermediate. In the first part of the growth phase gradient decreases to 1 nT/R_E, and B_z from 5 to 3–4 nT. During the second part gradient is close to zero, and B_z is stable.

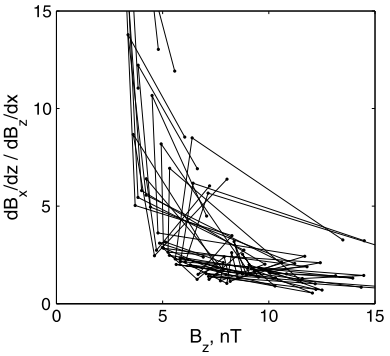

Fig. 17 Evolution of sheets in coordinates $(\partial B_x/\partial z)/(\partial B_z/\partial x)$, B_z. Figure is adopted from Petrukovich et al. (2013)

The sheet evolution from predominantly two-dimensional to predominantly one-dimensional structure can be followed in Fig. 17 (Petrukovich et al. 2013). For 10 cases with the stable positive gradient $\partial B_z/\partial x$ we show the dependence of the ratio $(\partial B_x/\partial z)/(\partial B_z/\partial x)$ on B_z. All events are close to the same hyperbolic-type curve. At the initial stage of thinning at $B_z \sim 5$–10 nT the ratio of the gradients is of the order 2–3. Upon further decrease of B_z below 5 nT vertical gradient increases sharply (CS intensifies).

Changes of magnetic field at the CS boundary, B_0, cannot be reliably monitored for such type of observations, however some estimates of dynamics of B_0/B_{ext} ratio can be obtained basing on general assumptions. Magnetic flux in a thin embedded CS with a thickness of the order of ion Larmor radius is $F_0 \sim 2$–$5 B_0 \rho = 0.006$–0.03 Wb/m (per unit width in y and proton temperature 4 keV), which is at least ten times less than the estimate of the total magnetic flux in the plasma sheet $F_{ext} \sim 0.4$–0.5 Wb/m at a distance from the Earth about 15 R_E (note, flux F_0 does not depend on B_0 because $\rho \sim 1/B_0$). Such a large difference in flux values imposes significant restrictions on possible B_0/B_{ext}. First of all, the minimal possible B_0/B_{ext} (minimal identifiable embedding) is set if current density in embedded and background sheets are equal: $B_0/L = B_{ext}/L_{ext}$. Converting this to magnetic flux units and neglecting all coefficients of the order of unity under the square root one could obtain:

$$(B_0/B_{ext})_{min} \sim \sqrt{F_0/F_{ext}} \tag{1}$$

Thus, for our statistics, the estimate $(B_0/B_{ext})_{min}$ is 0.2–0.3, which is consistent with observations (Fig. 6a, for example).

On the other hand, let us consider the opposite case with $B_0 \approx B_{ext}$, $F_0 \ll F_{ext}$. Then embedded sheet is a very thin plasma layer, in a thick background sheet, dominated by the magnetic pressure. Since the development of an embedded sheet begins during the growth phase within a sufficiently thick plasma sheet filled by hot and relatively dense plasma, such a configuration is unrealistic in the quiet magnetotail. During growth phases B_0/B_{ext} will be likely closer to $\sqrt{F_0/F_{ext}}$. After the onset a substantial part of plasma and magnetic flux are lost from the plasma sheet and $B_0 \approx B_{ext}$ is more feasible (Petrukovich et al. 2011). Configuration with $B_0 \approx B_{ext}$ is more likely also in the distant magnetotail, where F_{ext} is small.

9 Discussion and Conclusions

The availability of Cluster mission four-point data allowed for the first time to obtain information on spatial scales in the magnetotail on a regular basis and proceed with quantitative analysis of current sheet plasma physics as well as comparison with theoretical models.

Embedded configurations with thin intense CS inside a much wider plasma sheet were found to be typical for the magnetotail. Thickness of an embedded current density profile is about 1000–3000 km, which is only about 1–3 proton Larmor radii. Moreover, in the vicinity of the reconnection region one can expect to observe intense CSs with the thickness about a fraction of ρ (Nakamura et al. 2006, 2008; Artemyev et al. 2013a).

Effect of CS embedding manifests in ion kinetics. The strong increase of the current density without a comparable increase of the plasma density indicates that there is a small population of ions carrying significant cross-tail current. Such a population should have specific velocity distribution with the substantial asymmetry along the v_y direction. Indeed, detailed investigation of embedded CS reveals the beam-like ion distribution responsible for almost entire current density in embedded CS. Similar ion distributions were observed by THEMIS spacecraft (Zhou et al. 2009). The remaining plasma ($\sim$80–90 % of plasma density) can be considered as a background with a the uniform density profile across thin CS.

Oxygen ions (or high-temperature protons) influence CS structure. The increase of O^+ results in the increase of the CS thickness in agreement with modeling (Zelenyi et al. 2006). This effect confirms kinetic nature of CS and can play the important role in CS stability (Shay and Swisdak 2004; Markidis et al. 2011; Karimabadi et al. 2011; Liu et al. 2014).

The variations of ion (proton) and electron temperatures across CS are often more significant than the variations of plasma density. The scale of T_p variation is 2–10 times larger than the CS thickness. The development of some plasma instabilities (e.g., lower hybrid drift instability, drift kink/sausage instability) strongly depends on spatial gradients of the plasma density and/or temperature (Büchner and Kuska 1999; Daughton 1999a, 1999b, 2003; Yoon and Lui 2001; Tummel et al. 2014). Thus, in a realistic configuration these instabilities can be driven by the temperature gradients rather than by plasma density inhomogeneities.

Due to the small thickness of embedded CSs, ions are significantly demagnetized. The decoupling of ion and electron motions results in generation of polarization electrostatic field responsible for relatively strong cross-field electric drifts. Such drifts in weakly 2D configuration redistribute ion and electron contributions to the cross-tail current density in CSs with weak B_y and small $B_z \ll B_0$, making electron current comparable to the ion one. We conclude that electrostatic fields responsible for these drifts although very weak and hardly measurable are very important and should be included in any model pretending on realistic CS description.

Presence of the intense tilted sheets requires to reconsider criteria of general classification in the magnetotail. For example, the presence of intense currents $\sim$10–20 nA/m^2 cannot be considered as an direct indication of magnetotail reconfiguration before a substorm (Lui 2004), because these values of current density are typical for tilted CSs even in a quiet time.

Formation of thin CS during substorms reveals itself in three variables B_z, j_y, $\partial B_z/\partial x$. Substorm onsets (sheet instability) are associated with rather moderately intense current sheet (current density below 10 nA/m^2) and relatively small ratio B_0/B_{ext}. Much more intense current sheets are observed after onsets. This is a significant observational constraint for instability models. Predominantly two-dimensional structure with substantial gradients in X direction is gradually changing to predominantly one-dimensional with the negligible gradient along x-axis. Gradients along X play the critical role in many recent models of CS stability (Erkaev et al. 2009; Pritchett and Coroniti 2010; Sitnov and Schindler 2010, 2013; Pritchett and Coroniti 2013; Korovinskiy et al. 2013).

In summary, data collected by Cluster mission demonstrate that any accurate modelling of the magnetotail CS requires taking into account many specific properties: embedding, temperature gradients, polarization electrostatic field, redistribution of currents and the specific shape of ion distribution function containing beam-like features. All these effects can

influence CS stability and determine rate of magnetic reconnection (Burkhart et al. 1992b; Krallmann et al. 1994; Sitnov et al. 2002; Zelenyi et al. 2008, 2010; Karimabadi et al. 2003a, 2003b). Modern theories of stability concentrate on specific $B_z(x)$ profiles (Pritchett and Coroniti 2010, 2011; Sitnov and Schindler 2010; Sitnov et al. 2013), while many other CS properties are waiting for their comprehensive numerical modeling.

Some aspects of CS physics remain beyond this review and potential of Cluster data. First of all, we did not consider here B_y (shear) magnetic field component in CSs. For the majority of observed CSs this component is almost absent or very small $B_y \leq B_z$, but cases with $B_y \geq B_z$ are still abundant (Nakamura et al. 2008; Petrukovich 2009, 2011). Cluster observations have shown that the B_y component can be significantly enhanced by local field-aligned currents (Rong et al. 2012; Grigorenko et al. 2013). In this case, we may observe a parabolic profile of $B_y \sim 1 - (B_x/B_0)^2$ well described in theoretical models (Artemyev 2011; Mingalev et al. 2012; Vasko et al. 2014). However, the origin of such specific CS configuration with enhanced B_y is still unknown. In the events with a large magnetic shear component, field-aligned (rather than transverse) currents dominate, which are poorly addressed by existing theories. Moreover the theory of charged particle motion in CSs with B_y and a finite convection electric field E_y predicts the strong chaotization of ion trajectories and reduction of the cross-tail current (Artemyev et al. 2013b, 2014a), which is not readily observed. Thus, further experimental and theoretical investigation of CSs with intermediate B_y values ($|B_y| < B_0$) seems to be necessary.

While the vertical structure of the magnetotail CS is well investigated, the horizontal (along the tail) configuration is much less known. Cluster measurements of local B_z gradients in the near-Earth tail are not quite sufficient to restore the instantaneous profiles of crucial sheet characteristics (B_0, B_z, j_y) along X. Knowledge of these profiles is important for the identification of the most effective instability or select between specific sheet models. Only several statistical studies (Kan and Baumjohann 1990; Wang et al. 2009; Kissinger et al. 2012; Rong et al. 2014), are available now which considered averaged data collected during several years of spacecraft measurements. Potentially data necessary for reconstruction of the instantaneous CS configuration can be provided by five THEMIS spacecraft distributed along the magnetotail (Artemyev et al. 2013b).

The third important deficiency of our knowledge is insufficient understanding of electron current variability and structure of very thin and very intense CSs with domination of electron currents. It can be resolved only with future experiments having substantially better temporal and spatial resolutions such as the MMS, which is planned to be launched in 2015. It includes four spacecraft with separation 10–100 km, specially designed to study the electron physics in reconnecting current sheets. Cluster mission still remaining operative with in-depth investigation of 100–1000 km scales provide an important baseline for future studies.

Acknowledgements Work of A.A.P., A.V.A., I.Y.V. is supported by Russian Scientific Fund (project # 14-12-00824). R.N. is supported by the Austrian Science Fund (FWF I429-N16, P23862-N16).

References

V. Angelopoulos, C.F. Kennel, F.V. Coroniti, R. Pellat, H.E. Spence, M.G. Kivelson, R.J. Walker, W. Baumjohann, W.C. Feldman, J.T. Gosling, Characteristics of ion flow in the quiet state of the inner plasma sheet. Geophys. Res. Lett. **20**, 1711–1714 (1993). doi:10.1029/93GL00847

J. Arons, Pulsar wind nebulae as cosmic pevatrons: a current sheet's tale. Space Sci. Rev. **173**, 341–367 (2012). doi:10.1007/s11214-012-9885-1

A.V. Artemyev, A model of one-dimensional current sheet with parallel currents and normal component of magnetic field. Phys. Plasmas **18**(2), 022104 (2011). doi:10.1063/1.3552141

A.V. Artemyev, L.M. Zelenyi, Kinetic structure of current sheets in the Earth magnetotail. Space Sci. Rev. **178**, 419–440 (2013). doi:10.1007/s11214-012-9954-5

A.V. Artemyev, A.I. Neishtadt, L.M. Zelenyi, Ion motion in the current sheet with sheared magnetic field—Part 1: Quasi-adiabatic theory. Nonlinear Process. Geophys. **20**(1), 163–178 (2013a). doi:10.5194/npg-20-163-2013. http://www.nonlin-processes-geophys.net/20/163/2013/

A.V. Artemyev, A.I. Neishtadt, L.M. Zelenyi, Ion motion in the current sheet with sheared magnetic field—Part 2: Non-adiabatic effects. Nonlinear Process. Geophys. **20**, 899–919 (2013b). doi:10.5194/npg-20-899-2013

A.V. Artemyev, A.I. Neishtadt, L.M. Zelenyi, Rapid geometrical chaotization in slow-fast Hamiltonian systems. Phys. Rev. E **89**(6), 060902 (2014a). doi:10.1103/PhysRevE.89.060902

A.V. Artemyev, I.Y. Vasko, S. Kasahara, Thin current sheets in the Jovian magnetotail. Planet. Space Sci. **96**, 133–145 (2014b). doi:10.1016/j.pss.2014.03.012

A.V. Artemyev, A.A. Petrukovich, L.M. Zelenyi, H.V. Malova, V.Y. Popov, R. Nakamura, A. Runov, S. Apatenkov, Comparison of multi-point measurements of current sheet structure and analytical models. Ann. Geophys. **26**, 2749–2758 (2008)

A.V. Artemyev, A.A. Petrukovich, L.M. Zelenyi, R. Nakamura, H.V. Malova, V.Y. Popov, Thin embedded current sheets: cluster observations of ion kinetic structure and analytical models. Ann. Geophys. **27**, 4075–4087 (2009)

A.V. Artemyev, A.A. Petrukovich, R. Nakamura, L.M. Zelenyi, Proton velocity distribution in thin current sheets: cluster observations and theory of transient trajectories. J. Geophys. Res. **115**, 12255 (2010). doi:10.1029/2010JA015702

A.V. Artemyev, A.A. Petrukovich, R. Nakamura, L.M. Zelenyi, Cluster statistics of thin current sheets in the Earth magnetotail: specifics of the dawn flank, proton temperature profiles and electrostatic effects. J. Geophys. Res. **116**, 0923 (2011a). doi:10.1029/2011JA016801

A.V. Artemyev, W. Baumjohann, A.A. Petrukovich, R. Nakamura, I. Dandouras, A. Fazakerley, Proton/electron temperature ratio in the magnetotail. Ann. Geophys. **29**, 2253–2257 (2011b). doi:10.5194/angeo-29-2253-2011

A.V. Artemyev, A.A. Petrukovich, R. Nakamura, L.M. Zelenyi, Adiabatic electron heating in the magnetotail current sheet: cluster observations and analytical models. J. Geophys. Res. **117**, 06219 (2012). doi:10.1029/2012JA017513

A.V. Artemyev, A.A. Petrukovich, A.G. Frank, R. Nakamura, L.M. Zelenyi, Intense current sheets in the magnetotail: peculiarities of electron physics. J. Geophys. Res. **118**, 2789–2799 (2013a). doi:10.1002/jgra.50297

A.V. Artemyev, A.A. Petrukovich, R. Nakamura, L.M. Zelenyi, Profiles of electron temperature and B_z along Earth's magnetotail. Ann. Geophys. **31**, 1109–1114 (2013b). doi:10.5194/angeo-31-1109-2013

Y. Asano, T. Mukai, M. Hoshino, Y. Saito, H. Hayakawa, T. Nagai, Evolution of the thin current sheet in a substorm observed by Geotail. J. Geophys. Res. **108**, 1189 (2003). doi:10.1029/2002JA009785

Y. Asano, T. Mukai, M. Hoshino, Y. Saito, H. Hayakawa, T. Nagai, Current sheet structure around the near-Earth neutral line observed by Geotail. J. Geophys. Res. **109**, 2212 (2004a). doi:10.1029/2003JA010114

Y. Asano, T. Mukai, M. Hoshino, Y. Saito, H. Hayakawa, T. Nagai, Statistical study of thin current sheet evolution around substorm onset. J. Geophys. Res. **109**, 5213 (2004b). doi:10.1029/2004JA010413

M.J. Aschwanden, Particle acceleration and kinematics in solar flares—A synthesis of recent observations and theoretical concepts. Space Sci. Rev. **101**, 1–227 (2002). doi:10.1023/A:1019712124366

M. Ashour-Abdalla, J. Buechner, L.M. Zelenyi, The quasi-adiabatic ion distribution in the central plasma sheet and its boundary layer. J. Geophys. Res. **96**, 1601–1609 (1991). doi:10.1029/90JA01921

M. Ashour-Abdalla, J.P. Berchem, J. Buechner, L.M. Zelenyi, Shaping of the magnetotail from the mantle—Global and local structuring. J. Geophys. Res. **98**, 5651–5676 (1993). doi:10.1029/92JA01662

D.N. Baker, T.I. Pulkkinen, V. Angelopoulos, W. Baumjohann, R.L. McPherron, Neutral line model of substorms: past results and present view. J. Geophys. Res. **101**, 12975–13010 (1996). doi:10.1029/95JA03753

A. Balogh, C.M. Carr, M.H. Acuña, M.W. Dunlop, T.J. Beek, P. Brown, K. Fornaçon, E. Georgescu, K. Glassmeier, J. Harris, G. Musmann, T. Oddy, K. Schwingenschuh, The cluster magnetic field investigation: overview of in-flight performance and initial results. Ann. Geophys. **19**, 1207–1217 (2001). doi:10.5194/angeo-19-1207-2001

W. Baumjohann, G. Paschmann, C.A. Cattell, Average plasma properties in the central plasma sheet. J. Geophys. Res. **94**, 6597–6606 (1989). doi:10.1029/JA094iA06p06597

K.W. Behannon, L.F. Burlaga, N.F. Ness, The Jovian magnetotail and its current sheet. J. Geophys. Res. **86**, 8385–8401 (1981). doi:10.1029/JA086iA10p08385

M.K. Bird, D.B. Beard, The self-consistent geomagnetic tail under static conditions. Planet. Space Sci. **20**, 2057–2072 (1972). doi:10.1016/0032-0633(72)90062-1
J. Birn, Self-consistent magnetotail theory—General solution for the quiet tail with vanishing field-aligned currents. J. Geophys. Res. **84**, 5143–5152 (1979). doi:10.1029/JA084iA09p05143
J. Birn, E.R. Priest, *Reconnection of Magnetic Fields: Magnetohydrodynamics and Collisionless Theory and Observations* 2007
J. Birn, K. Schindler, M. Hesse, Thin electron current sheets and their relation to auroral potentials. J. Geophys. Res. **109**, 2217 (2004). doi:10.1029/2003JA010303
J. Birn, R. Sommer, K. Schindler, Open and closed magnetospheric tail configurations and their stability. Astrophys. Space Sci. **35**, 389–402 (1975). doi:10.1007/BF00637005
J. Büchner, J. Kuska, Sausage mode instability of thin current sheets as a cause of magnetospheric substorms. Ann. Geophys. **17**, 604–612 (1999). doi:10.1007/s005850050788
J. Büchner, L.M. Zelenyi, Regular and chaotic charged particle motion in magnetotaillike field reversals. I—Basic theory of trapped motion. J. Geophys. Res. **94**, 11821–11842 (1989). doi:10.1029/JA094iA09p11821
J.L. Burch, T.E. Moore, R.B. Torbert, B. Giles, MMS Overview and Science Objectives. Space Sci. Rev. (2014)
G.R. Burkhart, J. Chen, Particle motion in x-dependent Harris-like magnetotail models. J. Geophys. Res. **98**, 89–97 (1993). doi:10.1029/92JA01528
G.R. Burkhart, J.F. Drake, P.B. Dusenbery, T.W. Speiser, A particle model for magnetotail neutral sheet equilibria. J. Geophys. Res. **97**, 13799–13815 (1992a). doi:10.1029/92JA00495
G.R. Burkhart, J.F. Drake, P.B. Dusenbery, T.W. Speiser, Ion tearing in a magnetotail configuration with an embedded thin current sheet. J. Geophys. Res. **97**, 16749–16756 (1992b). doi:10.1029/92JA01523
S.W.H. Cowley, R. Pellat, A note on adiabatic solutions of the one-dimensional current sheet problem. Planet. Space Sci. **27**, 265–271 (1979). doi:10.1016/0032-0633(79)90069-2
J. Credland, G. Mecke, J. Ellwood, The cluster mission: ESA'S spacefleet to the magnetosphere. Space Sci. Rev. **79**, 33–64 (1997). doi:10.1023/A:1004914822769
W. Daughton, The unstable eigenmodes of a neutral sheet. Phys. Plasmas **6**, 1329–1343 (1999a). doi:10.1063/1.873374
W. Daughton, Two-fluid theory of the drift kink instability. J. Geophys. Res. **104**, 28701–28708 (1999b). doi:10.1029/1999JA900388
W. Daughton, Electromagnetic properties of the lower-hybrid drift instability in a thin current sheet. Phys. Plasmas **10**, 3103–3119 (2003). doi:10.1063/1.1594724
E.A. Davey, M. Lester, S.E. Milan, R.C. Fear, C. Forsyth, The orientation and current density of the magnetotail current sheet: a statistical study of the effect of geomagnetic conditions. J. Geophys. Res. **117**, 7217 (2012). doi:10.1029/2012JA017715
M.K. Dougherty, L.W. Esposito, S.M. Krimigis, *Saturn from Cassini-Huygens* 2009. doi:10.1007/978-1-4020-9217-6
M.W. Dunlop, A. Balogh, K.-H. Glassmeier, P. Robert, Four-point cluster application of magnetic field analysis tools: the curlometer. J. Geophys. Res. **107**, 1384 (2002). doi:10.1029/2001JA005088
J.W. Eastwood, Consistency of fields and particle motion in the 'Speiser' model of the current sheet. Planet. Space Sci. **20**, 1555–1568 (1972). doi:10.1016/0032-0633(72)90182-1
J.W. Eastwood, The warm current sheet model, and its implications on the temporal behaviour of the geomagnetic tail. Planet. Space Sci. **22**, 1641–1668 (1974). doi:10.1016/0032-0633(74)90108-1
N.V. Erkaev, V.S. Semenov, I.V. Kubyshkin, M.V. Kubyshkina, H.K. Biernat, MHD model of the flapping motions in the magnetotail current sheet. J. Geophys. Res. **114**, 3206 (2009). doi:10.1029/2008JA013728
C.P. Escoubet, M. Fehringer, M. Goldstein, Introduction: the cluster mission. Ann. Geophys. **19**, 1197–1200 (2001). doi:10.5194/angeo-19-1197-2001
P. Francfort, R. Pellat, Magnetic merging in collisionless plasmas. Geophys. Res. Lett. **3**, 433–436 (1976). doi:10.1029/GL003i008p00433
J.T. Gosling, Magnetic reconnection in the solar wind. Space Sci. Rev. **172**, 187–200 (2012). doi:10.1007/s11214-011-9747-2
E.E. Grigorenko, H.V. Malova, A.V. Artemyev, O.V. Mingalev, E.A. Kronberg, R. Koleva, P.W. Daly, J.B. Cao, J.-A. Sauvaud, C.J. Owen, L.M. Zelenyi, Current sheet structure and kinetic properties of plasma flows during a near-Earth magnetic reconnection under the presence of a guide field. J. Geophys. Res. **118**, 3265–3287 (2013). doi:10.1002/jgra.50310
G. Gustafsson, M. André, T. Carozzi, A.I. Eriksson, C.-G. Fälthammar, R. Grard, G. Holmgren, J.A. Holtet, N. Ivchenko, T. Karlsson, Y. Khotyaintsev, S. Klimov, H. Laakso, P.-A. Lindqvist, B. Lybekk, G. Marklund, F. Mozer, K. Mursula, A. Pedersen, B. Popielawska, S. Savin, K. Stasiewicz, P. Tanskanen, A. Vaivads, J.-E. Wahlund, First results of electric field and density observations by cluster EFW based on initial months of operation. Ann. Geophys. **19**, 1219–1240 (2001). doi:10.5194/angeo-19-1219-2001

E.G. Harris, On a plasma sheet separating regions of oppositely directed magnetic field. Nuovo Cimento **23**, 115–123 (1962)
M. Hoshino, A. Nishida, T. Mukai, Y. Saito, T. Yamamoto, S. Kokubun, Structure of plasma sheet in magnetotail: double-peaked electric current sheet. J. Geophys. Res. **101**, 24775–24786 (1996). doi:10.1029/96JA02313
P.L. Israelevich, A.I. Ershkovich, R. Oran, Current carriers in the bifurcated tail current sheet: ions or electrons? J. Geophys. Res. **113**, 4215 (2008). doi:10.1029/2007JA012541
C.M. Jackman, C.S. Arridge, N. André, F. Bagenal, J. Birn, M.P. Freeman, X. Jia, A. Kidder, S.E. Milan, A. Radioti, J.A. Slavin, M.F. Vogt, M. Volwerk, A.P. Walsh, Large-scale structure and dynamics of the magnetotails of Mercury, Earth, Jupiter and Saturn. Space Sci. Rev. **182**, 85–154 (2014). doi:10.1007/s11214-014-0060-8
A.D. Johnstone, C. Alsop, S. Burge, P.J. Carter, A.J. Coates, A.J. Coker, A.N. Fazakerley, M. Grande, R.A. Gowen, C. Gurgiolo, B.K. Hancock, B. Narheim, A. Preece, P.H. Sheather, J.D. Winningham, R.D. Woodliffe, Peace: a plasma electron and current experiment. Space Sci. Rev. **79**, 351–398 (1997). doi:10.1023/A:1004938001388
J.R. Kan, On the structure of the magnetotail current sheet. J. Geophys. Res. **78**, 3773–3781 (1973). doi:10.1029/JA078i019p03773
J.R. Kan, W. Baumjohann, Isotropized magnetic-moment equation of state for the central plasma sheet. Geophys. Res. Lett. **17**, 271–274 (1990). doi:10.1029/GL017i003p00271
H. Karimabadi, W. Daughton, P.L. Pritchett, D. Krauss-Varban, Ion-ion kink instability in the magnetotail: 1. Linear theory. J. Geophys. Res. **108**, 1400 (2003a). doi:10.1029/2003JA010026
H. Karimabadi, P.L. Pritchett, W. Daughton, D. Krauss-Varban, Ion-ion kink instability in the magnetotail: 2. Three-dimensional full particle and hybrid simulations and comparison with observations. J. Geophys. Res. **108**, 1401 (2003b). doi:10.1029/2003JA010109
H. Karimabadi, V. Roytershteyn, C.G. Mouikis, L.M. Kistler, W. Daughton, Flushing effect in reconnection: effects of minority species of oxygen ions. Planet. Space Sci. **59**, 526–536 (2011). doi:10.1016/j.pss.2010.07.014
C.F. Kennel, Magnetospheres of the planets. Space Sci. Rev. **14**, 511–533 (1973). doi:10.1007/BF00214759
J. Kissinger, R.L. McPherron, T.-S. Hsu, V. Angelopoulos, Diversion of plasma due to high pressure in the inner magnetosphere during steady magnetospheric convection. J. Geophys. Res. **117**, 5206 (2012). doi:10.1029/2012JA017579
D.B. Korovinskiy, A. Divin, N.V. Erkaev, V.V. Ivanova, I.B. Ivanov, V.S. Semenov, G. Lapenta, S. Markidis, H.K. Biernat, M. Zellinger, MHD modeling of the double-gradient (kink) magnetic instability. J. Geophys. Res. **118**, 1146–1158 (2013). doi:10.1002/jgra.50206
T. Krallmann, J. Dreher, K. Schindler, On the stability of the ion-tearing mode in equilibria with embedded thin current sheets, in *Int. Conf. Substorms*, 1994, pp. 499–503
A.P. Kropotkin, H.V. Malova, M.I. Sitnov, Self-consistent structure of a thin anisotropic current sheet. J. Geophys. Res. **102**, 22099–22106 (1997). doi:10.1029/97JA01316
Y.H. Liu, L.M. Kistler, C.G. Mouikis, V. Roytershteyn, H. Karimabadi, The scale of the magnetotail reconnecting current sheet in the presence of O^+. Geophys. Res. Lett. **41**, 4819–4827 (2014). doi:10.1002/2014GL060440
A.T.Y. Lui, Potential plasma instabilities for substorm expansion onsets. Space Sci. Rev. **113**, 127–206 (2004). doi:10.1023/B:SPAC.0000042942.00362.4e
S. Markidis, G. Lapenta, L. Bettarini, M. Goldman, D. Newman, L. Andersson, Kinetic simulations of magnetic reconnection in presence of a background O^+ population. J. Geophys. Res. (2011). doi:10.1029/2011JA016429
D.J. McComas, H.E. Spence, C.T. Russell, M.A. Saunders, The average magnetic field draping and consistent plasma properties of the Venus magnetotail. J. Geophys. Res. **91**, 7939–7953 (1986a). doi:10.1029/JA091iA07p07939
D.J. McComas, S.J. Bame, C.T. Russell, R.C. Elphic, The near-Earth cross-tail current sheet—detailed ISEE 1 and 2 case studies. J. Geophys. Res. **91**, 4287–4301 (1986b). doi:10.1029/JA091iA04p04287
D.J. McComas, J.T. Gosling, C.T. Russell, J.A. Slavin, Magnetotails at unmagnetized bodies—comparison of comet Giacobini–Zinner and Venus. J. Geophys. Res. **92**, 10111–10117 (1987). doi:10.1029/JA092iA09p10111
S. Minami, A.I. Podgornyi, I.M. Podgornyi, Laboratory evidence of earthward electric field in the magnetotail current sheet. Geophys. Res. Lett. **20**, 9–12 (1993). doi:10.1029/92GL02492
O.V. Mingalev, I.V. Mingalev, M.N. Mel'nik, A.V. Artemyev, H.V. Malova, V.Y. Popov, S. Chao, L.M. Zelenyi, Kinetic models of current sheets with a sheared magnetic field. Plasma Phys. Rep. **38**, 300–314 (2012). doi:10.1134/S1063780X12030063
D.G. Mitchell, D.J. Williams, C.Y. Huang, L.A. Frank, C.T. Russell, Current carriers in the near-Earth cross-tail current sheet during substorm growth phase. Geophys. Res. Lett. **17**, 583–586 (1990). doi:10.1029/GL017i005p00583

R. Nakamura, W. Baumjohann, A. Runov, Y. Asano, Thin current sheets in the magnetotail observed by cluster. Space Sci. Rev. **122**, 29–38 (2006). doi:10.1007/s11214-006-6219-1
R. Nakamura, W. Baumjohann, M. Fujimoto, Y. Asano, A. Runov, C.J. Owen, A.N. Fazakerley, B. Klecker, H. Rème, E.A. Lucek, M. Andre, Y. Khotyaintsev, Cluster observations of an ion-scale current sheet in the magnetotail under the presence of a guide field. J. Geophys. Res. **113**, 7 (2008). doi:10.1029/2007JA012760
N.F. Ness, The Earth's magnetic tail. J. Geophys. Res. **70**, 2989–3005 (1965). doi:10.1029/JZ070i013p02989
N.F. Ness, M.H. Acuna, L.F. Burlaga, J.E.P. Connerney, R.P. Lepping, Magnetic fields at Neptune. Science **246**, 1473–1478 (1989). doi:10.1126/science.246.4936.1473
E.N. Parker, Spontaneous current sheets in magnetic fields: with applications to stellar x-rays, in *Spontaneous Current Sheets in Magnetic Fields: with Applications to Stellar x-Rays*. International Series in Astronomy and Astrophysics, vol. 1 (Oxford University Press, New York, 1994)
G. Paschmann, S.J. Schwartz, *Issi Book on Analysis Methods for Multi-Spacecraft Data*. ESA Special Publication, vol. 449 2000
A.A. Petrukovich, Dipole tilt effects in plasma sheet by: statistical model and extreme values. Ann. Geophys. **27**, 1343–1352 (2009). doi:10.5194/angeo-27-1343-2009
A.A. Petrukovich, Origins of plasma sheet B_y. J. Geophys. Res. **116**, 7217 (2011). doi:10.1029/2010JA016386
A.A. Petrukovich, T. Mukai, S. Kokubun, S.A. Romanov, Y. Saito, T. Yamamoto, L.M. Zelenyi, Substorm-associated pressure variations in the magnetotail plasma sheet and lobe. J. Geophys. Res. **104**, 4501–4514 (1999). doi:10.1029/98JA02418
A.A. Petrukovich, W. Baumjohann, R. Nakamura, A. Balogh, T. Mukai, K.-H. Glassmeier, H. Reme, B. Klecker, Plasma sheet structure during strongly northward IMF. J. Geophys. Res. **108**, 1258 (2003). doi:10.1029/2002JA009738
A.A. Petrukovich, T.L. Zhang, W. Baumjohann, R. Nakamura, A. Runov, A. Balogh, C. Carr, Oscillatory magnetic flux tube slippage in the plasma sheet. Ann. Geophys. **24**, 1695–1704 (2006)
A.A. Petrukovich, W. Baumjohann, R. Nakamura, A. Runov, A. Balogh, H. Rème, Thinning and stretching of the plasma sheet. J. Geophys. Res. **112**, 10213 (2007). doi:10.1029/2007JA012349
A.A. Petrukovich, W. Baumjohann, R. Nakamura, A. Runov, Formation of current density profile in tilted current sheets. Ann. Geophys. **26**, 3669–3676 (2008)
A.A. Petrukovich, W. Baumjohann, R. Nakamura, H. Rème, Tailward and earthward flow onsets observed by cluster in a thin current sheet. J. Geophys. Res. **114**, 9203 (2009). doi:10.1029/2009JA014064
A.A. Petrukovich, A.V. Artemyev, H.V. Malova, V.Y. Popov, R. Nakamura, L.M. Zelenyi, Embedded current sheets in the Earth magnetotail. J. Geophys. Res. **116**, 1–25 (2011). doi:10.1029/2010JA015749
A.A. Petrukovich, A.V. Artemyev, R. Nakamura, E.V. Panov, W. Baumjohann, Cluster observations of dBz/dx during growth phase magnetotail stretching intervals. J. Geophys. Res. **118**, 5720–5730 (2013). doi:10.1002/jgra.50550
E. Priest, T. Forbes, *Magnetic Reconnection* 2000
P.L. Pritchett, F.V. Coroniti, A kinetic ballooning/interchange instability in the magnetotail. J. Geophys. Res. **115**, 06301 (2010). doi:10.1029/2009JA014752
P.L. Pritchett, F.V. Coroniti, Plasma sheet disruption by interchange-generated flow intrusions. Geophys. Res. Lett. **381**, 10102 (2011). doi:10.1029/2011GL047527
P.L. Pritchett, F.V. Coroniti, Structure and consequences of the kinetic ballooning/interchange instability in the magnetotail. J. Geophys. Res. **118**, 146–159 (2013). doi:10.1029/2012JA018143
H. Rème, C. Aoustin, J.M. Bosqued, I. Dandouras, B. Lavraud, J.A. Sauvaud, A. Barthe, J. Bouyssou, T. Camus, O. Coeur-Joly, A. Cros, J. Cuvilo, F. Ducay, Y. Garbarowitz, J.L. Medale, E. Penou, H. Perrier, D. Romefort, J. Rouzaud, C. Vallat, D. Alcaydé, C. Jacquey, C. Mazelle, C. D'Uston, E. Möbius, L.M. Kistler, K. Crocker, M. Granoff, C. Mouikis, M. Popecki, M. Vosbury, B. Klecker, D. Hovestadt, H. Kucharek, E. Kuenneth, G. Paschmann, M. Scholer, N. Sckopke, E. Seidenschwang, C.W. Carlson, D.W. Curtis, C. Ingraham, R.P. Lin, J.P. McFadden, G.K. Parks, T. Phan, V. Formisano, E. Amata, M.B. Bavassano-Cattaneo, P. Baldetti, R. Bruno, G. Chionchio, A. di Lellis, M.F. Marcucci, G. Pallocchia, A. Korth, P.W. Daly, B. Graeve, H. Rosenbauer, V. Vasyliunas, M. McCarthy, M. Wilber, L. Eliasson, R. Lundin, S. Olsen, E.G. Shelley, S. Fuselier, A.G. Ghielmetti, W. Lennartsson, C.P. Escoubet, H. Balsiger, R. Friedel, J. Cao, R.A. Kovrazhkin, I. Papamastorakis, R. Pellat, J. Scudder, B. Sonnerup, First multispacecraft ion measurements in and near the Earth's magnetosphere with the identical cluster ion spectrometry (CIS) experiment. Ann. Geophys. **19**, 1303–1354 (2001). doi:10.5194/angeo-19-1303-2001
F.J. Rich, V.M. Vasyliunas, R.A. Wolf, On the balance of stresses in the plasma sheet. J. Geophys. Res. **77**, 4670–4676 (1972). doi:10.1029/JA077i025p04670
Z.J. Rong, C. Shen, A.A. Petrukovich, W.X. Wan, Z.X. Liu, The analytic properties of the flapping current sheets in the Earth magnetotail. Planet. Space Sci. **58**, 1215–1229 (2010). doi:10.1016/j.pss.2010.04.016

Z.J. Rong, W.X. Wan, C. Shen, X. Li, M.W. Dunlop, A.A. Petrukovich, L.-N. Hau, T.L. Zhang, H. Rème, A.M. Du, E. Lucek, Profile of strong magnetic field B_y component in magnetotail current sheets. J. Geophys. Res. **117**, 6216 (2012). doi:10.1029/2011JA017402
Z.J. Rong, W.X. Wan, C. Shen, A.A. Petrukovich, W. Baumjohann, M.W. Dunlop, Y.C. Zhang, Radial distribution of magnetic field in Earth magnetotail current sheet. Planet. Space Sci. (2014). doi:10.1016/j.pss.2014.07.014
A. Runov, V.A. Sergeev, W. Baumjohann, R. Nakamura, S. Apatenkov, Y. Asano, M. Volwerk, Z. Vörös, T.L. Zhang, A. Petrukovich, A. Balogh, J. Sauvaud, B. Klecker, H. Rème, Electric current and magnetic field geometry in flapping magnetotail current sheets. Ann. Geophys. **23**, 1391–1403 (2005a)
A. Runov, V.A. Sergeev, R. Nakamura, W. Baumjohann, T.L. Zhang, Y. Asano, M. Volwerk, Z. Vörös, A. Balogh, H. Rème, Reconstruction of the magnetotail current sheet structure using multi-point cluster measurements. Planet. Space Sci. **53**, 237–243 (2005b). doi:10.1016/j.pss.2004.09.049
A. Runov, V.A. Sergeev, R. Nakamura, W. Baumjohann, S. Apatenkov, Y. Asano, T. Takada, M. Volwerk, Z. Vörös, T.L. Zhang, J. Sauvaud, H. Rème, A. Balogh, Local structure of the magnetotail current sheet: 2001 cluster observations. Ann. Geophys. **24**, 247–262 (2006)
K. Schindler, A self-consistent theory of the tail of the magnetosphere, in *Earth's Magnetospheric Processes*, ed. by B.M. McCormac Astrophysics and Space Science Library, vol. 32, 1972, p. 200
K. Schindler, A theory of the substorm mechanism. J. Geophys. Res. **79**, 2803–2810 (1974). doi:10.1029/JA079i019p02803
K. Schindler, Theories of tail structures. Space Sci. Rev. **23**, 365–374 (1979). doi:10.1007/BF00172245
K. Schindler, *Physics of Space Plasma Activity* (Cambridge University Press, Cambridge, 2006). doi:10.2277/0521858976
K. Schindler, J. Birn, Magnetotail theory. Space Sci. Rev. **44**, 307–355 (1986). doi:10.1007/BF00200819
K. Schindler, J. Birn, Models of two-dimensional embedded thin current sheets from Vlasov theory. J. Geophys. Res. **107**, 1193 (2002). doi:10.1029/2001JA000304
K. Schindler, J. Birn, M. Hesse, Kinetic model of electric potentials in localized collisionless plasma structures under steady quasi-gyrotropic conditions. Phys. Plasmas **19**(8), 082904 (2012). doi:10.1063/1.4747162
V.A. Sergeev, D.G. Mitchell, C.T. Russell, D.J. Williams, Structure of the tail plasma/current sheet at $\sim 11 R_E$ and its changes in the course of a substorm. J. Geophys. Res. **98**, 17345–17366 (1993). doi:10.1029/93JA01151
V.A. Sergeev, D.A. Sormakov, S.V. Apatenkov, W. Baumjohann, R. Nakamura, A.V. Runov, T. Mukai, T. Nagai, Survey of large-amplitude flapping motions in the midtail current sheet. Ann. Geophys. **24**, 2015–2024 (2006)
A.S. Sharma, R. Nakamura, A. Runov, E.E. Grigorenko, H. Hasegawa, M. Hoshino, P. Louarn, C.J. Owen, A. Petrukovich, J. Sauvaud, V.S. Semenov, V.A. Sergeev, J.A. Slavin, B.U.Ö Sonnerup, L.M. Zelenyi, G. Fruit, S. Haaland, H. Malova, K. Snekvik, Transient and localized processes in the magnetotail: a review. Ann. Geophys. **26**, 955–1006 (2008)
M.A. Shay, M. Swisdak, Three-species collisionless reconnection: effect of O^+ on magnetotail reconnection. Phys. Rev. Lett. **93**(17), 175001 (2004). doi:10.1103/PhysRevLett.93.175001
C. Shen, Z.X. Liu, X. Li, M. Dunlop, E. Lucek, Z.J. Rong, Z.Q. Chen, C.P. Escoubet, H.V. Malova, A.T.Y. Lui, A. Fazakerley, A.P. Walsh, C. Mouikis, Flattened current sheet and its evolution in substorms. J. Geophys. Res. **113**, 7 (2008). doi:10.1029/2007JA012812
M.I. Sitnov, K. Schindler, Tearing stability of a multiscale magnetotail current sheet. Geophys. Res. Lett. **37**, 8102 (2010). doi:10.1029/2010GL042961
M.I. Sitnov, L.M. Zelenyi, H.V. Malova, A.S. Sharma, Thin current sheet embedded within a thicker plasma sheet: self-consistent kinetic theory. J. Geophys. Res. **105**, 13029–13044 (2000). doi:10.1029/1999JA000431
M.I. Sitnov, A.S. Sharma, P.N. Guzdar, P.H. Yoon, Reconnection onset in the tail of Earth's magnetosphere. J. Geophys. Res. **107**, 1256 (2002). doi:10.1029/2001JA009148
M.I. Sitnov, M. Swisdak, P.N. Guzdar, A. Runov, Structure and dynamics of a new class of thin current sheets. J. Geophys. Res. **111**, 8204 (2006). doi:10.1029/2005JA011517
M.I. Sitnov, N. Buzulukova, M. Swisdak, V.G. Merkin, T.E. Moore, Spontaneous formation of dipolarization fronts and reconnection onset in the magnetotail. Geophys. Res. Lett. **40**, 22–27 (2013). doi:10.1029/2012GL054701
J.A. Slavin, B.J. Anderson, D.N. Baker, M. Benna, S.A. Boardsen, R.E. Gold, G.C. Ho, S.M. Imber, H. Korth, S.M. Krimigis, R.L. McNutt Jr., J.M. Raines, M. Sarantos, D. Schriver, S.C. Solomon, P. Trávníček, T.H. Zurbuchen, MESSENGER and Mariner 10 flyby observations of magnetotail structure and dynamics at Mercury. J. Geophys. Res. **117**, 1215 (2012). doi:10.1029/2011JA016900
E.J. Smith, L. Davis Jr., D.E. Jones, P.J. Coleman Jr., D.S. Colburn, P. Dyal, C.P. Sonett, A.M.A. Frandsen, The planetary magnetic field and magnetosphere of Jupiter: pioneer 10. J. Geophys. Res. **79**, 3501 (1974). doi:10.1029/JA079i025p03501

K. Snekvik, E. Tanskanen, N. Østgaard, L. Juusola, K. Laundal, E.I. Gordeev, A.L. Borg, Changes in the magnetotail configuration before near-Earth reconnection. J. Geophys. Res. **117**, 2219 (2012). doi:10.1029/2011JA017040

T.W. Speiser, Particle trajectories in model current sheets, 1, analytical solutions. J. Geophys. Res. **70**, 4219–4226 (1965). doi:10.1029/JZ070i017p04219

T.W. Speiser, Particle trajectories in model current sheets, 2, applications to auroras using a geomagnetic tail model. J. Geophys. Res. **72**, 3919–3932 (1967). doi:10.1029/JZ072i015p03919

L.C. Steinhauer, M.P. McCarthy, E.C. Whipple, Multifluid model of a one-dimensional steady state magnetotail current sheet. J. Geophys. Res. **113**, 4207 (2008). doi:10.1029/2007JA012578

K. Tummel, L. Chen, Z. Wang, X.Y. Wang, Y. Lin, Gyrokinetic theory of electrostatic lower-hybrid drift instabilities in a current sheet with guide field. Phys. Plasmas **21**(5), 052104 (2014). doi:10.1063/1.4875720

O.L. Vaisberg, L.M. Zeleny, Formation of the plasma mantle in the Venusian magnetosphere. Icarus **58**, 412–430 (1984). doi:10.1016/0019-1035(84)90087-3

I.Y. Vasko, A.V. Artemyev, V.Y. Popov, H.V. Malova, Kinetic models of two-dimensional plane and axially symmetric current sheets: group theory approach. Phys. Plasmas **20**(2), 022110 (2013). doi:10.1063/1.4792263

I.Y. Vasko, A.V. Artemyev, A.A. Petrukovich, R. Nakamura, L.M. Zelenyi, The structure of strongly tilted current sheets in the Earth magnetotail. Ann. Geophys. **32**, 133–146 (2014a). doi:10.5194/angeo-32-133-2014

I.Y. Vasko, L.M. Zelenyi, A.V. Artemyev, A.A. Petrukovich, H.V. Malova, T.L. Zhang, A.O. Fedorov, V.Y. Popov, S. Barabash, R. Nakamura, The structure of the Venusian current sheet. Planet. Space Sci. **96**, 81–89 (2014b). doi:10.1016/j.pss.2014.03.013

I.Y. Vasko, A.V. Artemyev, A.A. Petrukovich, H.V. Malova, Thin current sheets with strong bell-shape guide field: cluster observations and models with beams. Ann. Geophys. **32**(10), 1349–1360 (2014). doi:10.5194/angeo-32-1349-2014. http://www.ann-geophys.net/32/1349/2014/

C. Wang, L.R. Lyons, R.A. Wolf, T. Nagai, J.M. Weygand, A.T.Y. Lui, Plasma sheet $PV^{5/3}$ and nV and associated plasma and energy transport for different convection strengths and AE levels. J. Geophys. Res. **114**, 1–2 (2009). doi:10.1029/2008JA013849

E. Whipple, R. Puetter, M. Rosenberg, A two-dimensional, time-dependent, near-Earth magnetotail. Adv. Space Res. **11**, 133–142 (1991). doi:10.1016/0273-1177(91)90024-E

B. Wilken, P.W. Daly, U. Mall, K. Aarsnes, D.N. Baker, R.D. Belian, J.B. Blake, H. Borg, J. Büchner, M. Carter, J.F. Fennell, R. Friedel, T.A. Fritz, F. Gliem, M. Grande, K. Kecskemety, G. Kettmann, A. Korth, S. Livi, S. McKenna-Lawlor, K. Mursula, B. Nikutowski, C.H. Perry, Z.Y. Pu, J. Roeder, G.D. Reeves, E.T. Sarris, I. Sandahl, F. Søraas, J. Woch, Q.-G. Zong, First results from the RAPID imaging energetic particle spectrometer on board cluster. Ann. Geophys. **19**, 1355–1366 (2001). doi:10.5194/angeo-19-1355-2001

P.H. Yoon, A.T.Y. Lui, On the drift-sausage mode in one-dimensional current sheet. J. Geophys. Res. **106**, 1939–1948 (2001). doi:10.1029/2000JA000130

P.H. Yoon, A.T.Y. Lui, Model of ion- or electron-dominated current sheet. J. Geophys. Res. **109**, 11213 (2004). doi:10.1029/2004JA010555

P.H. Yoon, A.T.Y. Lui, A class of exact two-dimensional kinetic current sheet equilibria. J. Geophys. Res. **110**, 1202 (2005). doi:10.1029/2003JA010308

L.M. Zelenyi, A.V. Artemyev, A.A. Petrukovich, Earthward electric field in the magnetotail: cluster observations and theoretical estimates. Geophys. Res. Lett. **37**, 6105 (2010). doi:10.1029/2009GL042099

L.M. Zelenyi, M.I. Sitnov, H.V. Malova, A.S. Sharma, Thin and superthin ion current sheets. quasi-adiabatic and nonadiabatic models. Nonlinear Process. Geophys. **7**, 127–139 (2000)

L.M. Zelenyi, H.V. Malova, V.Y. Popov, D. Delcourt, A.S. Sharma, Nonlinear equilibrium structure of thin currents sheets: influence of electron pressure anisotropy. Nonlinear Process. Geophys. **11**, 579–587 (2004)

L.M. Zelenyi, H.V. Malova, V.Y. Popov, D.C. Delcourt, N.Y. Ganushkina, A.S. Sharma, "Matreshka" model of multilayered current sheet. Geophys. Res. Lett. **33**, 5105 (2006). doi:10.1029/2005GL025117

L.M. Zelenyi, A.V. Artemyev, H.V. Malova, V.Y. Popov, Marginal stability of thin current sheets in the Earth's magnetotail. J. Atmos. Sol.-Terr. Phys. **70**, 325–333 (2008). doi:10.1016/j.jastp.2007.08.019

L.M. Zelenyi, A.V. Artemyev, K.V. Malova, A.A. Petrukovich, R. Nakamura, Metastability of current sheets. Phys. Usp. **53**, 933–941 (2010). doi:10.3367/UFNe.0180.201009g.0973

L.M. Zelenyi, H.V. Malova, A.V. Artemyev, V.Y. Popov, A.A. Petrukovich, Thin current sheets in collisionless plasma: equilibrium structure, plasma instabilities, and particle acceleration. Plasma Phys. Rep. **37**, 118–160 (2011). doi:10.1134/S1063780X1102005X

L.M. Zelenyi, A.I. Neishtadt, A.V. Artemyev, D.L. Vainchtein, H.V. Malova, Quasiadiabatic dynamics of charged particles in a space plasma. Phys. Usp. **56**, 347–394 (2013). doi:10.3367/UFNe.0183.201304b.0365

T.L. Zhang, W. Baumjohann, R. Nakamura, A. Balogh, K. Glassmeier, A wavy twisted neutral sheet observed by CLUSTER. Geophys. Res. Lett. **29**(19), 190000 (2002). doi:10.1029/2002GL015544

X. Zhou, V. Angelopoulos, A. Runov, M.I. Sitnov, F. Coroniti, P. Pritchett, Z.Y. Pu, Q. Zong, J.P. McFadden, D. Larson, K. Glassmeier, Thin current sheet in the substorm late growth phase: modeling of THEMIS observations. J. Geophys. Res. **114**, 3223 (2009). doi:10.1029/2008JA013777